

## INFORMATION TO USERS

This manuscript has been reproduced from the microfilm master. UMI films the text directly from the original or copy submitted. Thus, some thesis and dissertation copies are in typewriter face, while others may be from any type of computer printer.

The quality of this reproduction is dependent upon the quality of the copy submitted. Broken or indistinct print, colored or poor quality illustrations and photographs, print bleedthrough, substandard margins, and improper alignment can adversely affect reproduction.

In the unlikely event that the author did not send UMI a complete manuscript and there are missing pages, these will be noted. Also, if unauthorized copyright material had to be removed, a note will indicate the deletion.

Oversize materials (e.g., maps, drawings, charts) are reproduced by sectioning the original, beginning at the upper left-hand corner and continuing from left to right in equal sections with small overlaps. Each original is also photographed in one exposure and is included in reduced form at the back of the book.

Photographs included in the original manuscript have been reproduced xerographically in this copy. Higher quality 6" x 9" black and white photographic prints are available for any photographs or illustrations appearing in this copy for an additional charge. Contact UMI directly to order.

# U·M·I

University Microfilms International  
A Bell & Howell Information Company  
300 North Zeeb Road, Ann Arbor, MI 48106-1346 USA  
313/761-4700 800/521-0600



**Order Number 1348475**

**Calculation of transmission line parameters for multiconductor  
lines in a multi-dielectric medium**

**McFarland, Robert Bynum, M.S.**

**The University of Arizona, 1992**

**U·M·I**

300 N. Zeeb Rd.  
Ann Arbor, MI 48106



CALCULATION OF TRANSMISSION LINE PARAMETERS FOR  
MULTICONDUCTOR LINES IN A MULTI-DIELECTRIC MEDIUM

by

Robert Bynum McFarland

---

A Thesis Submitted to the Faculty of the  
DEPARTMENT OF ELECTRICAL AND COMPUTER ENGINEERING  
In Partial Fulfillment of the Requirements  
For the Degree of  
MASTER OF SCIENCE  
WITH A MAJOR IN ELECTRICAL ENGINEERING  
In the Graduate College  
THE UNIVERSITY OF ARIZONA

1 9 9 2

## STATEMENT BY AUTHOR


This thesis has been submitted in partial fulfillment of requirements for an advanced degree at The University of Arizona and is deposited in the University Library to be made available to borrowers under rules of the Library.

Brief quotations from this thesis are allowable without special permission, provided that accurate acknowledgment of source is made. Requests for permission for extended quotation from or reproduction of this manuscript in whole or in part may be granted by the head of the major department or the Dean of the Graduate College when in his or her judgment the proposed use of the material is in the interests of scholarship. In all other instances, however, permission must be obtained from the author.

SIGNED: 

## APPROVAL BY THESIS DIRECTOR

This thesis has been approved on the date shown below:



Andreas Cangelaris  
Professor of Electrical and Computer Engineering

5/1/92

Date

*To Hollie, Brenna and Maz*

## ACKNOWLEDGEMENTS

I would like to thank my advisor Dr. Andreas C. Cangellaris for his encouragement and technical advice which made this thesis possible. I am also grateful to my thesis committee members, Dr. John R. Brews and Dr. Steven L. Dvorak for their constructive suggestions. I would also like to express my thanks to my friends in the Center for Electronic Packaging Research, Alex Mou, Mike Gibbons Ramesh Senthinathan, Pochang Hsu and Basel Al-Masri for their moral support.



## TABLE OF CONTENTS

<b>LIST OF FIGURES.....</b>	<b>7</b>
<b>LIST OF TABLES.....</b>	<b>9</b>
<b>ABSTRACT.....</b>	<b>10</b>
<b>1 Introduction.....</b>	<b>11</b>
1.1 Transmission Line Models and the Characterization of VLSI inter-connections .....	11
1.1.1 Cross Talk .....	13
1.1.2 Attenuation And Propagation Velocity .....	13
1.2 Quasi-TEM Analysis .....	14
<b>2 The Integral Equation Method.....</b>	<b>16</b>
2.1 Integral Equation Solution to Poisson's Equation .....	16
2.2 Spectral Domain Green's Function for a Multi-Layered Medium ....	21
2.3 Asymptotic Form of the Spectral Domain Green's Function .....	33
2.4 Numerical Comparison of the Spectral Domain Green's Functions ..	39
2.5 Space Domain Green's Function .....	50
<b>3 Numerical Solution of the Integral Equation.....</b>	<b>52</b>
3.1 Method of Moments solution for the Charge Distribution .....	52
3.2 Calculation of the Per Unit Length Capacitance, Inductance and Conductance Matrices .....	67
<b>4 Numerical Results.....</b>	<b>70</b>
4.1 MTL in a Uniform Layered Medium .....	70
4.2 Dielectric Coated Wires .....	72

4.3 Dielectric Coated Microstrip Line .....	74
4.4 Differential Lines in the Presence of a Vertical Dielectric Interface ..	74
<b>5 Computation Time .....</b>	<b>77</b>
5.1 CPU time Comparison Between Methods .....	77
<b>6 Conclusions and Future Directions .....</b>	<b>81</b>
<b>APPENDIX A The Exponential Integral .....</b>	<b>83</b>
<b>APPENDIX B The Cosine Integral .....</b>	<b>84</b>
<b>APPENDIX C Numerical Evaluation of Singular Integrals .....</b>	<b>86</b>
<b>REFERENCES .....</b>	<b>88</b>

## LIST OF FIGURES

1.1	Lumped Transmission Line Model .....	12
1.2	Two conductor transmission lines .....	12
2.1	Integration Paths for the Two-Layered Dielectric Medium .....	18
2.2	Cross section of a MTL in an Arbitrary Dielectric Medium .....	22
2.3	Source Point Embedded in a Single Dielectric Later .....	24
2.4	General Layered Dielectric Medium .....	26
2.5	Single Dielectric Boundary Between the Source and Observation Points.....	34
2.6	Four Slowest Decaying Attenuated Waves .....	37
2.7	Outward Directed waves Emanating from the Source at $d_k$ .....	38
2.8	Layered medium used in the comparison of the spectral domain Green's function and its asymptotic approximation.....	40
2.9	Spectral domain Green's function compared with the four wave asymptotic approximation .....	41
2.10	Spectral domain Green's function compared with the three wave asymptotic approximation .....	42
2.11	Spectral domain Green's function compared with the two wave asymp- totic approximation .....	43
2.12	Spectral domain Green's function compared with a single wave asymp- totic approximation .....	44
2.13	Effect of positive coordinate scaling on $k_T$ .....	45
2.14	Effect of negative coordinate scaling on $k_T$ .....	46
2.15	Layered medium with a thin layer between the source and observa- tion points.....	47
2.16	Four attenuated waves with the shortest pathlengths .....	48
2.17	Comparison between asymptotic approximations constructed from different attenuated waves .....	49

3.1	Cross Section of General Discretized Geometry .....	53
3.2	Unit Pulse Function .....	54
3.3	Layered geometry for analytic and asymptotic spectral domain Green's function comparisons .....	57
3.4	Comparison of the derivatives for the analytic and asymptotic spec- tral domain Green's functions .....	58
3.5	Arbitrary Dielectric Interface.....	61
3.6	Geometry relating $\Delta c$ and the observation point $P$ .....	63
4.1	Three Conducting Lines in a Three Layered Medium .....	71
4.2	Two-wire Ribbon .....	73
4.3	Dielectric Coated Microstrip Line .....	74
4.4	Differential lines in the presence of a vertical dielectric interface....	75
5.1	Single Conducting Line in a Multilayered Medium .....	78
5.2	Comparison of number of unknowns between methods .....	79
5.3	Comparison of CPU time between methods .....	80

## LIST OF TABLES

4.1	Results for the MTL in a Uniform Layered Medium Example. ....	72
4.2	Results for Two-wire Ribbon with and without the dielectric coating present .....	73
4.3	Results for the Microstrip Line with and without the dielectric coating	74
4.4	Results for the Differential Lines with and without DIELECTRIC 2 present .....	76

## ABSTRACT

A method for computing the per-unit-length capacitance matrix and the inductance matrix for multiconductor transmission lines in a multi-dielectric medium is presented. The multi-dielectric medium consists of both planar and non-planar dielectric regions. The formulation is based on an integral equation method for the free charge distribution on conductor surfaces and the polarization charge distribution on the non-planar dielectric-dielectric interfaces. The kernel of the integral equation is a space domain Green's function for a layered medium. The numerical solution is obtained by the method of moments.

## CHAPTER 1

### Introduction

There has recently been much effort in the calculation of parameters for multi-conductor transmission lines (MTL) embedded in a layered dielectric media. Previous efforts modeling MTL's in a planar multilayered medium have ranged from the quasi-static or quasi-TEM approximations to rigorous full-wave analysis [1-5]. The objective here is to extend the quasi-TEM analysis to MTL's in a more complicated multi-dielectric medium consisting of planar and non-planar dielectric interfaces.

#### 1.1 Transmission Line Models and the Characterization of VLSI interconnections

The study of electrical interconnections in electronic packaging is based on transmission line theory. Using transmission line theory, we may evaluate electrical performance of packages in terms of coupling noise, reflections, attenuation and propagation velocity. General transmission line models are completely described in terms of the per unit length (p.u.l.) parameters  $L$ ,  $C$ ,  $R$  and  $G$ . The lumped transmission line model for a single line, valid for  $\Delta z \ll \lambda$ , is shown in Figure 1.1

The expressions describing the voltage and current waveforms along an MTL under time-harmonic excitation are given by

$$\frac{d}{dz}[V] - \{[R] + j\omega[L]\}[I] = 0 \quad (1.1)$$

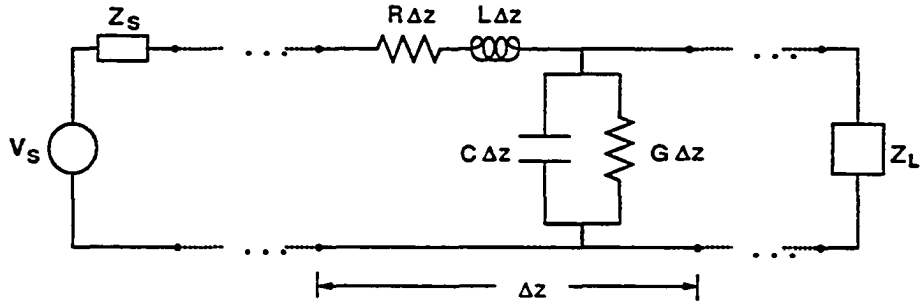


Figure 1.1: Lumped Transmission Line Model

$$\frac{d}{dz}[I] - \{[G] + j\omega[C]\}[V] = 0 \quad (1.2)$$

where  $[L]$  is the p.u.l. inductance matrix,  $[C]$  is the p.u.l. capacitance matrix,  $[R]$  is the p.u.l. resistance matrix and  $[G]$  is the p.u.l. conductance matrix. The resistance and conductance matrices represent conductor and dielectric losses, respectively.  $[V]$  and  $[I]$  are the voltage and current vectors.

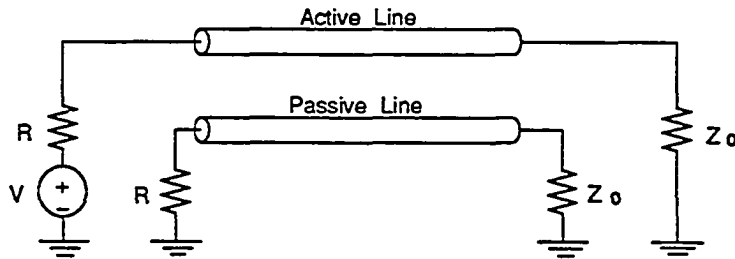


Figure 1.2: Two conductor transmission lines

Let us consider a two conductor interconnection in order to discuss the general characteristics of a MTL interconnection. In this system, one line is active



while the other is passive. The transmission line circuit for the pair is shown in Figure 1.2. Using this two conductor model, we will review the following transmission line properties.

### 1.1.1 Cross Talk

Coupling noise, or cross talk, is caused by electromagnetic coupling of signal lines. In terms of our two line model, the active line is capacitively coupled to the passive line by  $C_{12}$  and inductively coupled by  $L_{12}$ . The capacitive and inductive coupling coefficients are  $k_C = C_{12}/C_{11}$  and  $k_L = L_{12}/L_{11}$ , respectively. If  $k_C > k_L$  then capacitive coupling dominates and if  $k_L > k_C$ , then inductive coupling dominates. If  $k_C = k_L$ , there is little or no crosstalk. This may be seen by examining the expression for the forward traveling wave on the passive line at  $x=d$  [6]. This is

$$U_{fD}(t) = \frac{T_D}{2}(k_C - k_L)\frac{d}{dt}V_{s0}(t - T_D) \quad (1.3)$$

where  $T_D$  is the delay time required for a wave to travel from the driver to the receiver and  $V_{s0}(t) = V_s(t, x = 0)$ . From this expression, we see that  $U_{fD}(t) = 0$  when  $k_C = k_L$ . However (1.3) is only an approximation, so there may still be some crosstalk even when  $k_C = k_L$ . Finally, a word about reflections. Reflections are due to impedance mismatches between the transmission line and its terminations. In certain cases, these reflections may increase the crosstalk between lines.

### 1.1.2 Attenuation And Propagation Velocity

The attenuation constants and propagation velocities of our line are determined by solving the following eigenvalue problem [6]

$$\text{Det}[\gamma^2 \mathbf{1} - \mathbf{ZY}] = 0 \quad (1.4)$$

where  $\mathbf{1}$  is the identity matrix,  $\mathbf{Z} = [R] + j\omega[L]$  and  $\mathbf{Y} = [G] + j\omega[C]$ . Solving the eigenvalue problem, we obtain the eigenvalues  $\gamma_1$  and  $\gamma_2$  for the modes supported by the MTL. These are complex eigenvalues where the real part represents the attenuation constant and the imaginary part is the propagation constant for each mode. From the propagation constants, one may determine the propagation velocities for the  $N$  modes of an  $N$ -conductor MTL.

## 1.2 Quasi-TEM Analysis

In the quasi-TEM approximation of electromagnetic wave propagation in uniform MTL's, Maxwell's equations reduce to solving Poisson's equation in the zero frequency limit with the appropriate boundary conditions. Although conformal mapping techniques may be used to obtain analytical solutions of Poisson's equation for simple two dimensional transmission line configurations, complicated geometries including many conductors and dielectric-dielectric interfaces require numerical methods. Among these are the integral equation methods [1] [2], the variational method [4], the finite difference and the finite element methods [5].

The method used here is the integral equation method. In order to accommodate a medium consisting of both planar and non-planar dielectrics, the kernel of the integral equation is the space domain Green's function for a layered medium [2]. With this formulation, the boundary conditions at the interfaces between infinite parallel layers are built into the Green's function. Since we do not determine the polarization charge at these boundaries, the number of unknowns may be greatly reduced. Since this choice of Green's function is not consistent with boundary conditions at non-planar dielectric interfaces, the bound charge at these interfaces is introduced as an additional unknown.

The capacitance matrix is defined electrostatically by

$$[Q] = [C][V] \quad (1.5)$$

where  $[Q]$  is the total charge vector,  $[C]$  is the capacitance matrix and  $[V]$  is the potential vector. Our integral equation is based on the formulation for the potential at  $\mathbf{r}$  due to some system of charged conductors in a multi-dielectric medium. Taking the  $i^{th}$  equation of (1.5), we have

$$Q_i = \sum_{j=1}^N C_{ij} V_j, \quad i = 1, \dots, N \quad (1.6)$$

where  $N$  is the number of conducting lines. From (1.6), we see that the capacitance matrix element  $C_{ij}$  represents the total charge on the  $i^{th}$  conductor due to the potential of 1 volt on the  $j^{th}$  conductor while all other lines are grounded. By alternately setting one conductor to 1 volt and grounding all others, we use (1.5) to determine all elements of the capacitance matrix. The diagonal elements of the capacitance matrix represents the direct capacitance of an active line in the presence of a ground plane plus the mutual capacitances between the active line and all other grounded lines [10].

## CHAPTER 2

### The Integral Equation Method

The calculation of the per unit length capacitance, inductance and conductance matrices for uniform multiconductor transmission lines requires the p.u.l. surface electric charge distribution on the conductors embedded in a multi-dielectric medium. This charge distribution may be determined from the solution of the integral equation for the electrostatic potential in terms of the charge distribution and an appropriate Green's function.

#### 2.1 Integral Equation Solution to Poisson's Equation

Consider the general two dimensional electrostatic problem where we seek a solution for potential  $\phi(\mathbf{r})$  corresponding to some distribution of charge  $\rho$ . The Poisson equation is

$$\nabla \cdot (\epsilon(\mathbf{r}) \nabla \phi(\mathbf{r})) = -\rho(\mathbf{r}) \quad (2.1)$$

We can obtain a solution for  $\phi(\mathbf{r})$  by solving the Green's function problem. This amounts to solving Poisson's equation for a point source located at  $\mathbf{r}'$ .

$$\nabla \cdot (\epsilon(\mathbf{r}) \nabla G(\mathbf{r}|\mathbf{r}')) = -\delta(\mathbf{r} - \mathbf{r}') \quad (2.2)$$

Thus the Green's function represents the potential at some observation point  $\mathbf{r}$  due to a point source located at  $\mathbf{r}'$ . The medium for which we will construct

the Green's function is a multi-layered dielectric region. The Green's function will satisfy the appropriate boundary conditions at the interfaces between infinite dielectric layers. Defining  $S$  as the area of the domain and  $C$  as the boundary of  $S$ , we apply Green's theorem for  $\phi$  and  $G$  in a two dimensional sense to obtain

$$\begin{aligned} & \int_S [\phi(\mathbf{r}) \nabla \cdot (\epsilon(\mathbf{r}) \nabla G(\mathbf{r}|\mathbf{r}')) - G(\mathbf{r}|\mathbf{r}') \nabla \cdot (\epsilon(\mathbf{r}) \nabla \phi(\mathbf{r}))] da \\ &= \int_C (\phi(\mathbf{r}) \epsilon(\mathbf{r}) \nabla G(\mathbf{r}|\mathbf{r}') - G(\mathbf{r}|\mathbf{r}') \epsilon(\mathbf{r}) \nabla \phi(\mathbf{r})) \cdot \hat{n} dl \end{aligned} \quad (2.3)$$

For the dielectric geometries of interest, the right hand side term of (2.3) will reduce to zero. Consider the region of Figure (2.1). Here we have two dielectric regions  $S_1$  and  $S_2$ , where  $S = S_1 + S_2$ . These regions are bounded by  $C_1 = \Gamma_1 + \Gamma_1^\infty$  and  $C_2 = \Gamma_2 + \Gamma_2^\infty$ , respectively. For this region, we write

$$\begin{aligned} & \int_S [\phi(\mathbf{r}) \nabla \cdot (\epsilon(\mathbf{r}) \nabla G(\mathbf{r}|\mathbf{r}')) - G(\mathbf{r}|\mathbf{r}') \nabla \cdot (\epsilon(\mathbf{r}) \nabla \phi(\mathbf{r}))] da \\ &= \int_{C_1} (\phi(\mathbf{r}) \epsilon_1 \nabla G_1(\mathbf{r}|\mathbf{r}') - G_1(\mathbf{r}|\mathbf{r}') \epsilon_1 \nabla \phi(\mathbf{r})) \cdot \hat{n}_1 dl \\ &+ \int_{C_2} (\phi(\mathbf{r}) \epsilon_2 \nabla G_2(\mathbf{r}|\mathbf{r}') - G_2(\mathbf{r}|\mathbf{r}') \epsilon_2 \nabla \phi(\mathbf{r})) \cdot \hat{n}_2 dl \end{aligned} \quad (2.4)$$

In the limit as  $\delta y \rightarrow 0$ , we have

$$\begin{aligned} & \int_{\Gamma_1} (\phi(\mathbf{r}) \epsilon_1 \nabla G_1(\mathbf{r}|\mathbf{r}') - G_1(\mathbf{r}|\mathbf{r}') \epsilon_1 \nabla \phi(\mathbf{r})) \cdot \hat{n}_1 dl \\ &+ \int_{\Gamma_2} (\phi(\mathbf{r}) \epsilon_2 \nabla G_2(\mathbf{r}|\mathbf{r}') - G_2(\mathbf{r}|\mathbf{r}') \epsilon_2 \nabla \phi(\mathbf{r})) \cdot \hat{n}_2 dl \end{aligned}$$

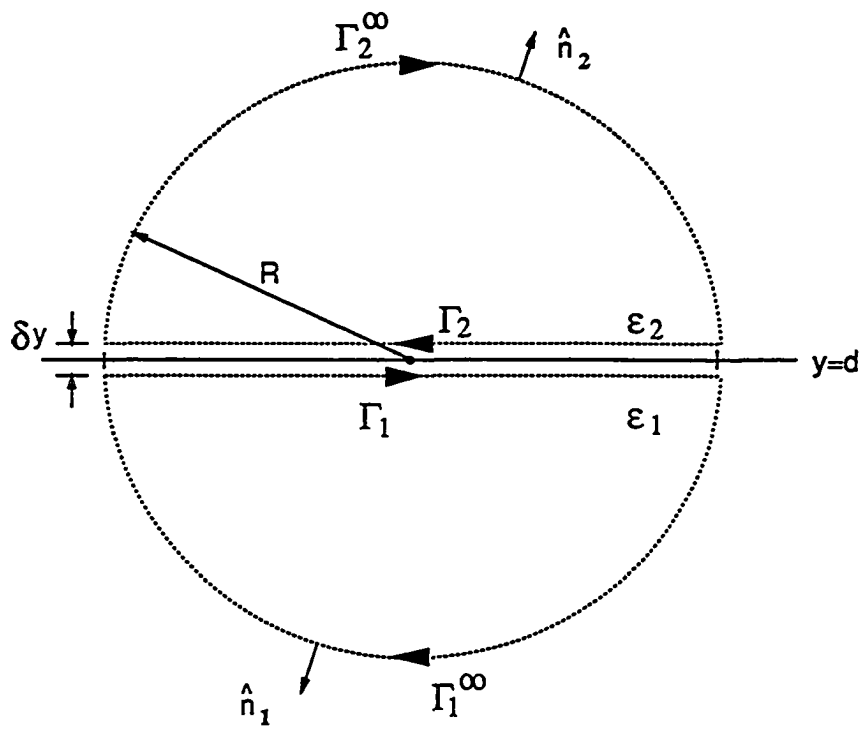


Figure 2.1: Integration Paths for the Two-Layered Dielectric Medium

$$\begin{aligned}
&= \int_{-\infty}^{\infty} \{(\phi(\mathbf{r})\epsilon_1 \nabla G_1(\mathbf{r}|\mathbf{r}') - G_1(\mathbf{r}|\mathbf{r}')\epsilon_1 \nabla \phi(\mathbf{r})) \\
&\quad - (\phi(\mathbf{r})\epsilon_2 \nabla G_2(\mathbf{r}|\mathbf{r}') - G_2(\mathbf{r}|\mathbf{r}')\epsilon_2 \nabla \phi(\mathbf{r}))\} \cdot \hat{n}_1 dl
\end{aligned} \tag{2.5}$$

where  $\hat{n} = \hat{n}_1$ . At the interface  $y = d$ , we have continuity of the potential and the normal component of the electric flux.

$$\phi(d^+) = \phi(d^-) \tag{2.6}$$

$$\epsilon_1 \frac{\partial \phi(\mathbf{r})}{\partial n} \Big|_{d^-} = \epsilon_2 \frac{\partial \phi(\mathbf{r})}{\partial n} \Big|_{d^+} \tag{2.7}$$

By forcing (2.5) to zero, we recover the following boundary conditions for the Green's function at a dielectric interface.

$$G_1|_d = G_2|_d \tag{2.8}$$

$$\epsilon_1 \frac{\partial G_1}{\partial n} \Big|_d = \epsilon_2 \frac{\partial G_2}{\partial n} \Big|_d \tag{2.9}$$

Let us now evaluate the integral over  $\Gamma_1^\infty$  in the limit  $R \rightarrow \infty$ . The boundary condition on the normal component of the electric flux as  $R \rightarrow \infty$  is zero, hence

$$\begin{aligned}
&\lim_{R \rightarrow \infty} \int_{\Gamma_1^\infty} \{\phi(\mathbf{r}) \nabla G_1(\mathbf{r}|\mathbf{r}') - G_1(\mathbf{r}|\mathbf{r}') \nabla \phi(\mathbf{r})\} \cdot \hat{n} dl \\
&= \lim_{R \rightarrow \infty} \int_{\Gamma_1^\infty} \phi(\mathbf{r}) \frac{\partial G_1}{\partial n} dl
\end{aligned} \tag{2.10}$$

By forcing this expression to zero, we obtain the boundary conditions on  $G_1$  at infinity. If we apply the same analysis in region 2 for  $G_2$ , we obtain the general boundary condition on the Green's function at infinity

$$\lim_{R \rightarrow \infty} \frac{\partial G}{\partial n} = 0 \quad (2.11)$$

Therefore, the integrals in (2.4) over  $C_1$  and  $C_2$  are zero and we are left with the expression

$$\int_S [\phi(\mathbf{r}) \nabla \cdot (\epsilon(\mathbf{r}) \nabla G(\mathbf{r}|\mathbf{r}')) - G(\mathbf{r}|\mathbf{r}') \nabla \cdot (\epsilon(\mathbf{r}) \nabla \phi(\mathbf{r}))] da = 0 \quad (2.12)$$

or, in view of (2.1) and (2.2)

$$\int_S \phi(\mathbf{r}) \delta(\mathbf{r} - \mathbf{r}') da = \int_S \rho(\mathbf{r}) G(\mathbf{r}|\mathbf{r}') da \quad (2.13)$$

Where the left hand side is simply  $\phi(\mathbf{r}')$ .

If we take advantage of reciprocity for the Green's function [8], that is  $G(\mathbf{r}|\mathbf{r}') = G(\mathbf{r}'|\mathbf{r})$ , we may interchange  $\mathbf{r}$  and  $\mathbf{r}'$  and obtain the following integral equation.

$$\phi(\mathbf{r}) = \int_S \rho(\mathbf{r}') G(\mathbf{r}|\mathbf{r}') da \quad (2.14)$$

Let us examine now the types of geometries we would like to consider. These are cross sections of multiconductor transmission lines contained in a multi-dielectric medium with both planar and non-planar dielectric interfaces. This generalized geometry is shown in Figure 2.2. Here,  $N_c$  represents the total number of conductors present, of which  $N_1$  are active and  $N_2$  are grounded. If  $N$  is the total number of conductors and non-planar dielectric interfaces, then  $N - N_c$  is



the number of non-planar dielectric boundaries in the chosen geometry. There are also  $N_d$  planar dielectric boundaries for which we will construct a space domain Green's function for each layer [2]. Non-planar dielectric interfaces will be treated using polarization charge as an additional unknown.

Given a system of  $N_c$  charged conductors, where the charge distribution resides on the surface of each conductor, the integral equation becomes

$$\phi(\mathbf{r}) = \sum_{i=1}^{N_c} \int_{C_i} \sigma_i(\mathbf{r}') G(\mathbf{r}|\mathbf{r}') d\mathbf{l}' \quad (2.15)$$

From this expression, the surface charge distribution will be determined for the  $j^{th}$  conductor raised to a potential of 1 volt while all others are grounded. Note however that the Green's function is determined only for a layered medium. When non-planar regions are also included, the effects of these dielectric discontinuities on the conductor surface charge distribution must be accounted for.

Before we construct our solution of the Green's function for the layered medium, we should note that the individual layers are considered infinite and uniform in the  $x$ -direction. In the next section, we will take advantage of this and construct a solution in the spectral domain. The green's function is then recovered by taking the inverse transform of the function in the spectral domain.

## 2.2 Spectral Domain Green's Function for a Multi-Layered Medium

The dielectric layers of the medium are considered uniform in the  $x$ -direction. Therefore, the Green's functions  $x$  dependence will be the absolute value of the difference in the  $x$  components of the source and observation points. The Green's function will be assumed to correspond to the potential at the observation point  $(x, y)$  due to a line source at  $(0, y')$  [2]. For this reason, we may use the Fourier cosine transform to define a spectral domain Green's function  $\tilde{G}$  which

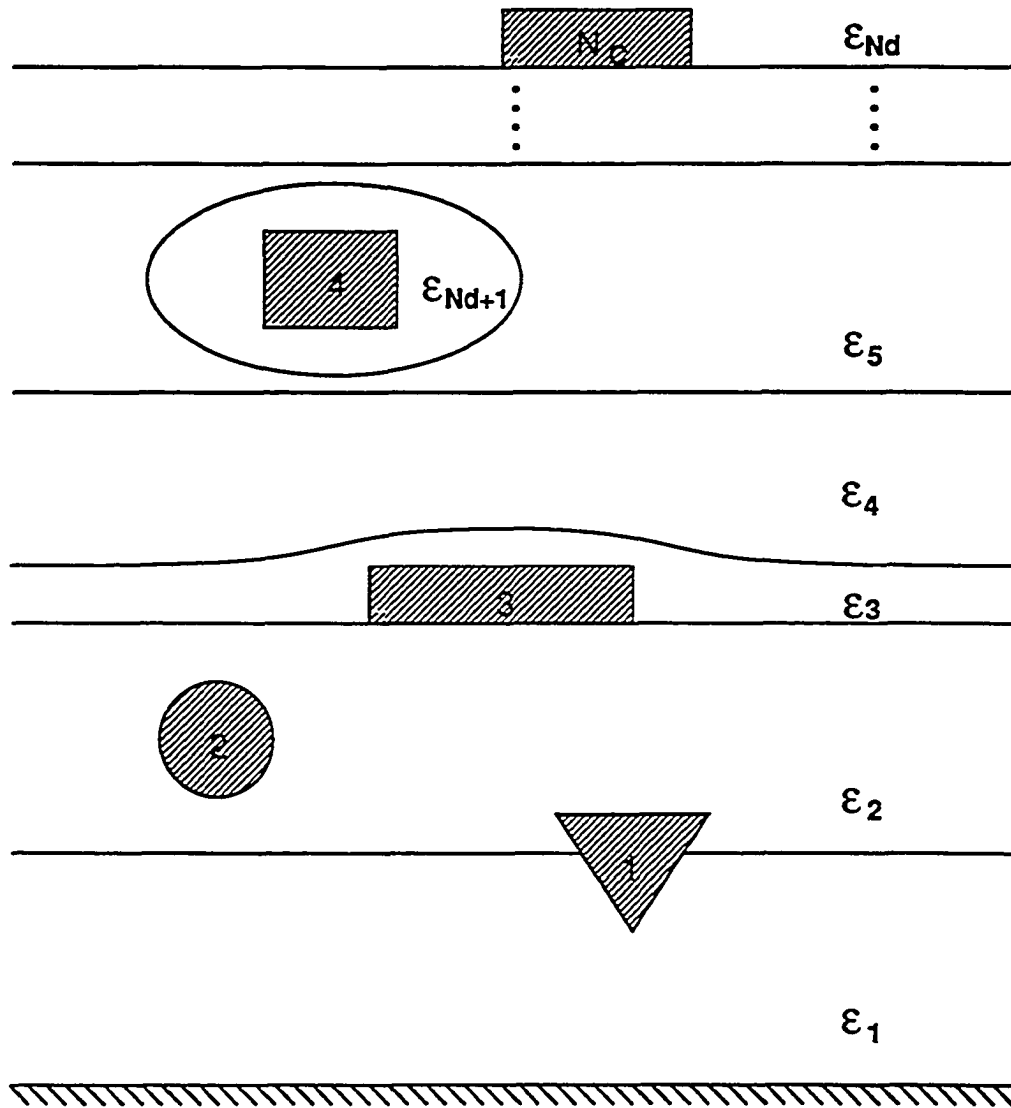


Figure 2.2: Cross section of a MTL in an Arbitrary Dielectric Medium

is independent of  $x$ . Note that the cosine transform is used instead of other forms of the Fourier transform for two reasons. First, it is even symmetric about  $x = x'$  so that the inverse Fourier transform provides a space domain Green's function for which the reciprocity theorem holds. Second, the interval of integration is  $[0, \infty]$ , as opposed to  $[-\infty, \infty]$  for the standard form of the Fourier transform. This will simplify the numerical evaluation of the Green's function at the observation point  $\mathbf{r}$ .

$$\tilde{G}(k_x, y|y') = \frac{1}{\pi} \int_0^\infty G(\mathbf{r}|\mathbf{r}') \cos[k_x(x - x')] dx \quad (2.16)$$

where  $\mathbf{r}$  locates the observation point,  $\mathbf{r}'$  locates the source point,  $G(\mathbf{r}|\mathbf{r}')$  is the Green's function and  $\tilde{G}(k_x, y|y')$  represents the spectral domain Green's function which is independent of  $x$ . We can write our Green's function  $G(\mathbf{r}|\mathbf{r}')$  in terms of the inverse Fourier cosine transform of  $\tilde{G}(k_x, y|y')$ .

$$G(\mathbf{r}|\mathbf{r}') = \frac{1}{\pi} \int_0^\infty \tilde{G}(k_x, y|y') \cos[k_x(x - x')] dk_x \quad (2.17)$$

If the above expression is to be useful, we must know the spectral domain Green's function everywhere in the medium. Equation (2.2) can be rewritten as follows.

$$\nabla^2 G(\mathbf{r}|\mathbf{r}') = -\delta(x - x')\delta(y - y') \quad (2.18)$$

Substituting (2.17) into (2.18) for  $G(\mathbf{r}|\mathbf{r}')$ , we write

$$\begin{aligned} \nabla^2 G(\mathbf{r}|\mathbf{r}') &= \frac{1}{\pi} \int_0^\infty \nabla^2 \{ \tilde{G} \cos[k_x(x - x')] \} dk_x \\ &= \frac{1}{\pi} \int_0^\infty \left\{ \frac{\partial^2}{\partial y^2} - k_x^2 \right\} \tilde{G} \cos[k_x(x - x')] dk_x \end{aligned}$$

$$= -\delta(x - x')\delta(y - y') \quad (2.19)$$

But the delta function  $\delta(x - x')$  can be expressed in the form

$$\delta(x - x') = \frac{1}{\pi} \int_0^\infty \cos[k_x(x - x')] dk_x \quad (2.20)$$

Comparing (2.20) with (2.19), we write the one dimensional Green's function problem as

$$\left\{ \frac{\partial^2}{\partial y^2} - k_x^2 \right\} \tilde{G} = -\delta(y - y') \quad (2.21)$$

From which we shall solve for the spectral domain Green's function  $\tilde{G}$ .

Now let us look at a single dielectric layer for an example of how the solution of the one-dimensional Green's function problem is constructed. Figure 2.3 shows a point source, located at  $y'$ , embedded in a dielectric layer.

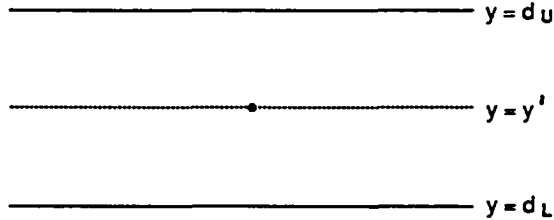


Figure 2.3: Source Point Embedded in a Single Dielectric Layer

The solution of the one-dimensional Green's function problem is of the form

$$\tilde{G}(k_x, y|y') = \begin{cases} Ae^{k_x y} + Be^{-k_x y} & y < y' \\ Ce^{k_x y} + De^{-k_x y} & y > y' \end{cases} \quad (2.22)$$

The coefficients A,B,C,D are found by applying boundary conditions at  $y = d_U$  and  $y = d_L$ . Henceforth, we will assume the source is located on the boundary between two dielectric layers. This is considered general since if the source lies within a uniform layer, we divide the layer into two layers of the same dielectric. Thus for the  $i^{th}$  layer, the solution of  $\tilde{G}$  is

$$\tilde{G}_i = A_i e^{k_x y} + B_i e^{-k_x y} \quad (2.23)$$

for  $i = 1, 2, \dots, N_d$ . All  $A_i, B_i$  are determined by applying a jump condition at the source location  $y = y'$  and boundary conditions at all other interfaces.

The domain in which we seek  $\tilde{G}$  is a simple layered dielectric medium. The possible cases include an infinite ground plane at  $y = 0$ , an additional ground plane above  $y = 0$ , and the case of ground at infinity. Figure 2.4 shows the layered dielectric structure without regard to how the first and last layers are terminated. Furthermore the arbitrary location of the source is denoted as the boundary  $d_k$ .

Boundary conditions are now applied at the  $i^{th}$  interface,  $i \neq k$ . These conditions are continuity of the potential and of the normal electric displacement vector. Since  $\tilde{G}$  represents the potential due to a point source located at  $y = d_k$ , these boundary conditions are written as

$$\tilde{G}_i(k_x, d_i | d_k) = \tilde{G}_{i+1}(k_x, d_i | d_k) \quad (2.24)$$

$$\epsilon_i \frac{\partial \tilde{G}}{\partial y} \Big|_{y=d_i} = \epsilon_{i+1} \frac{\partial \tilde{G}_{i+1}}{\partial y} \Big|_{y=d_i} \quad (2.25)$$

Inserting equation (2.23) into the above boundary conditions, we obtain

$$A_i e^{k_x d_i} + B_i e^{-k_x d_i} = A_{i+1} e^{k_x d_i} + B_{i+1} e^{-k_x d_i} \quad (2.26)$$

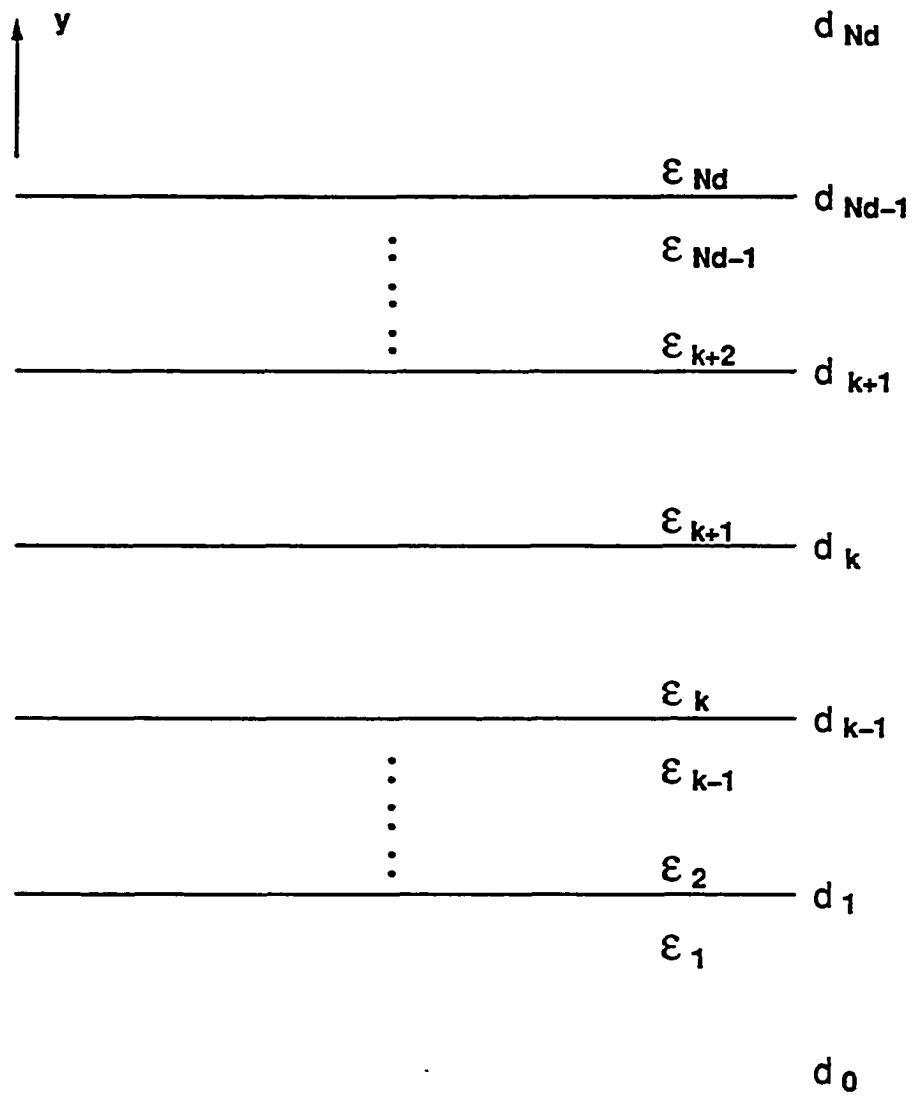


Figure 2.4: General Layered Dielectric Medium

$$\epsilon_{ri} [A_i e^{k_x d_i} - B_i e^{-k_x d_i}] = \epsilon_{ri+1} [A_{i+1} e^{k_x d_i} - B_{i+1} e^{-k_x d_i}] \quad (2.27)$$

Multiplying (2.26) and (2.27) by  $e^{k_x d_i}$  yields

$$A_i e^{2k_x d_i} + B_i = A_{i+1} e^{2k_x d_i} + B_{i+1} \quad (2.28)$$

$$\epsilon_{ri} [A_i e^{2k_x d_i} - B_i] = \epsilon_{ri+1} [A_{i+1} e^{2k_x d_i} - B_{i+1}] \quad (2.29)$$

Now if we multiply (2.28) by  $\epsilon_{ri}$  and then both add and subtract the result with (2.29), we have

$$A_i e^{2k_x d_i} = a_i A_{i+1} e^{2k_x d_i} + b_i B_{i+1} \quad (2.30)$$

$$B_i = b_i A_{i+1} e^{2k_x d_i} + a_i B_{i+1} \quad (2.31)$$

where

$$a_i = \frac{\epsilon_{ri} + \epsilon_{ri+1}}{2\epsilon_{ri}} \quad (2.32)$$

$$b_i = \frac{\epsilon_{ri} - \epsilon_{ri+1}}{2\epsilon_{ri}} \quad (2.33)$$

Similarly, if we multiply (2.28) by  $\epsilon_{ri+1}$ , then add and subtract the result with (2.29), we find

$$A_{i+1} = c_i A_i + h_i B_i e^{-2k_x d_i} \quad (2.34)$$

$$B_{i+1} = h_i e^{2k_z d_i} A_i + c_i B_i \quad (2.35)$$

where

$$c_i = \frac{\epsilon_{ri+1} + \epsilon_{ri}}{2\epsilon_{ri+1}} \quad (2.36)$$

$$h_i = \frac{\epsilon_{ri+1} - \epsilon_{ri}}{2\epsilon_{ri+1}} \quad (2.37)$$

Finally, if we multiply the  $A_{i+1}$  terms of equations (2.30) and (2.31) and the  $B_{i+1}$  terms of equations (2.34) and (2.35) by  $e^{2k_z d_{i+1}} e^{-2k_z d_{i+1}} = 1$ , we obtain the following matrix expressions.

$$\begin{bmatrix} A_i e^{2k_z d_i} \\ B_i \end{bmatrix} = U_i \begin{bmatrix} A_{i+1} e^{2k_z d_{i+1}} \\ B_{i+1} \end{bmatrix} \quad i \neq j \quad (2.38)$$

$$\begin{bmatrix} A_{i+1} \\ B_{i+1} e^{-2k_z d_{i+1}} \end{bmatrix} = L_i \begin{bmatrix} A_i \\ B_i e^{-2k_z d_i} \end{bmatrix} \quad i \neq j \quad (2.39)$$

where

$$U_i = \begin{bmatrix} a_i e^{-2k_z(d_{i+1}-d_i)} & b_i \\ b_i e^{-2k_z(d_{i+1}-d_i)} & a_i \end{bmatrix} \quad (2.40)$$

$$L_i = \begin{bmatrix} c_i & h_i \\ h_i e^{-2k_z(d_{i+1}-d_i)} & c_i e^{-2k_z(d_{i+1}-d_i)} \end{bmatrix} \quad (2.41)$$



Once the boundary conditions at  $d_0$  and  $d_{Nd}$  are known, one uses equations (2.38) and (2.39) in a top down or bottom up procedure to determine  $A_{k+1}, B_{k+1}$  in terms of  $A_{Nd}, B_{Nd}$  and  $A_k, B_k$  in terms of  $A_1, B_1$ . The coefficients  $A_1, B_1, A_{Nd}$  and  $B_{Nd}$  are then solved for by applying continuity of the potential and the normal electric displacement vector jump condition at the interface  $y = d_k$  where the source resides. These are

$$\tilde{G}_i(k_x, d_k | d_k) = \tilde{G}_{i+1}(k_x, d_k | d_k) \quad (2.42)$$

$$\epsilon_{i+1} \frac{\partial \tilde{G}_{i+1}}{\partial y} \Big|_{y=d_k} - \epsilon_i \frac{\partial \tilde{G}_i}{\partial y} \Big|_{y=d_k} = -1 \quad (2.43)$$

Or, more specifically

$$A_k e^{k_x d_k} + B_k e^{-k_x d_k} = A_{i+1} e^{k_x d_k} + B_{k+1} e^{-k_x d_k} \quad (2.44)$$

$$\epsilon_{r,k+1} [A_{k+1} e^{k_x d_k} - B_{k+1} e^{-k_x d_k}] - \epsilon_{r,k} [A_k e^{k_x d_k} - B_k e^{-k_x d_k}] = -\frac{1}{\epsilon_0 k_x} \quad (2.45)$$

To demonstrate the calculation of these coefficients, let us consider the simple case where an infinite conducting ground plane is positioned at  $y = 0$  and the uppermost layer extends to infinity. For this case, we begin by noting that from boundary conditions applied at  $y = 0$  and  $y = \infty$ , we have

$$A_1 = -B_1 \quad (2.46)$$

$$A_{Nd} = 0 \quad (2.47)$$

Using equation (2.38), we begin a top down procedure to obtain  $A_{k+1}, B_{k+1}$  in terms of  $B_{Nd}$ .

$$\underline{i = Nd - 1}$$

$$\begin{bmatrix} A_{Nd-1} e^{2k_z d_{Nd-1}} \\ B_{Nd-1} \end{bmatrix} = U_{Nd-1} \begin{bmatrix} 0 \\ B_{Nd} \end{bmatrix}$$

$$\underline{i = Nd - 2}$$

$$\begin{bmatrix} A_{Nd-2} e^{2k_z d_{Nd-2}} \\ B_{Nd-2} \end{bmatrix} = U_{Nd-2} \begin{bmatrix} A_{Nd-1} e^{2k_z d_{Nd-1}} \\ B_{Nd-1} \end{bmatrix} = U_{Nd-2} U_{Nd-1} \begin{bmatrix} 0 \\ B_{Nd} \end{bmatrix}$$

$$\vdots$$

$$\underline{i = k + 1}$$

$$\begin{bmatrix} A_{k+1} e^{2k_z d_{k+1}} \\ B_{k+1} \end{bmatrix} = \prod_{i=k+1}^{Nd-1} U_i \begin{bmatrix} 0 \\ B_{Nd} \end{bmatrix} \quad (2.48)$$

which we can express in the more practical form

$$\begin{bmatrix} A_{k+1} e^{2k_z d_{k+1}} \\ B_{k+1} \end{bmatrix} = \begin{bmatrix} U_{11} & U_{12} \\ U_{21} & U_{22} \end{bmatrix} \begin{bmatrix} 0 \\ B_{Nd} \end{bmatrix} \quad (2.49)$$

where all  $U_{ij}$  are known.

Similarly, using equation (2.39), we can perform a bottom up procedure to obtain  $A_k, B_k$  in terms of  $A_1$ .

$$\underline{i = 1}$$

$$\begin{aligned}
& \begin{bmatrix} A_2 \\ B_2 e^{-2k_x d_2} \end{bmatrix} = \mathbf{L}_1 \begin{bmatrix} A_1 \\ -A_1 e^{-2k_x d_1} \end{bmatrix} \\
& \quad \underline{i = 2} \\
& \begin{bmatrix} A_3 \\ B_3 e^{-2k_x d_3} \end{bmatrix} = \mathbf{L}_2 \begin{bmatrix} A_2 \\ B_2 e^{-2k_x d_2} \end{bmatrix} = \mathbf{L}_2 \mathbf{L}_1 \begin{bmatrix} A_1 \\ -A_1 e^{-2k_x d_1} \end{bmatrix} \\
& \quad \vdots \\
& \quad \underline{i = k - 1} \\
& \begin{bmatrix} A_k \\ B_k e^{-2k_x d_k} \end{bmatrix} = \prod_{i=1}^{k-1} \mathbf{L}_{k-i} \begin{bmatrix} A_1 \\ -A_1 e^{-2k_x d_1} \end{bmatrix} \tag{2.50}
\end{aligned}$$

which again can be expressed in the more practical form

$$\begin{bmatrix} A_k \\ B_k e^{-2k_x d_k} \end{bmatrix} = \begin{bmatrix} L_{11} & L_{12} \\ L_{21} & L_{22} \end{bmatrix} \begin{bmatrix} A_1 \\ -A_1 e^{-2k_x d_1} \end{bmatrix} \tag{2.51}$$

where all  $L_{ij}$  are known.

At this point, we would like to apply equations (2.44) and (2.45) to solve for  $A_1$  and  $B_{Nd}$ . Since this is a system of two equations and two unknowns, let us write these as

$$aA_1 + bB_{Nd} = 0 \tag{2.52}$$

$$cA_1 + dB_{Nd} = -\frac{e^{-k_x d_k}}{\epsilon_0 k_x} \quad (2.53)$$

Which we can express in the matrix form

$$\begin{bmatrix} a & b \\ c & d \end{bmatrix} \begin{bmatrix} A_1 \\ B_{Nd} \end{bmatrix} = \begin{bmatrix} 0 \\ -e^{-k_x d_k} / \epsilon_0 k_x \end{bmatrix} \quad (2.54)$$

Expressions for the terms  $a, b, c$  and  $d$  will be obtained in the following analysis. Expanding (2.49) and (2.51) into their four equations, we obtain

$$A_k = A_1(L_{11} - L_{12}e^{-2k_x d_1}) = \xi_1 A_1 \quad (2.55)$$

$$B_k e^{-2k_x d_k} = A_1(L_{21} - L_{22}e^{-2k_x d_1}) = \xi_2 A_1 \quad (2.56)$$

$$A_{k+1} e^{2k_x d_{k+1}} = U_{12} B_{Nd} = \xi_3 B_{Nd} \quad (2.57)$$

$$B_{k+1} = U_{22} B_{Nd} = \xi_4 B_{Nd} \quad (2.58)$$

which defines  $\xi_1, \xi_2, \xi_3$  and  $\xi_4$ . If we apply the above expressions to our boundary equations at  $y = d_k$ , we find that

$$a = \xi_1 + \xi_2 \quad (2.59)$$

$$b = -(\xi_3 e^{-2k_x d_{k+1}} + \xi_4 e^{-2k_x d_k}) \quad (2.60)$$

$$c = \xi_2 - \xi_1 \quad (2.61)$$

$$d = \xi_3 e^{-2k_x d_{k+1}} - \xi_4 e^{-2k_x d_k} \quad (2.62)$$

Finally, solving (2.54), we obtain the following expressions for  $A_1$  and  $B_{N_d}$ .

$$A_1 = \frac{b e^{-k_x d_k}}{k_x \epsilon_0 (ad - bc)} \quad (2.63)$$

$$B_{N_d} = -\frac{a e^{-k_x d_k}}{k_x \epsilon_0 (ad - bc)} \quad (2.64)$$

Once  $A_1$  and  $B_{N_d}$  are known, all remaining  $a_i, B_i$  are determined by repeated use of equations (2.38) and (2.39).

### 2.3 Asymptotic Form of the Spectral Domain Green's Function

The need for an asymptotic approximation of the spectral domain Green's function arises as we attempt to take the inverse Fourier transform to recover the space domain Green's function. Substituting (2.23) into (2.17), we have

$$G(\mathbf{r}|\mathbf{r}') = \frac{1}{\pi} \int_0^\infty (A_{m+1} e^{k_x y} + B_{m+1} e^{-k_x y}) \cos[k_x (x - x')] dk_x \quad (2.65)$$

However, we see right away that the integral of the growing exponential over  $[0, \infty]$  will present problems. To illustrate this, consider a uniform medium above an infinite ground plane. The coefficients of the spectral domain Green's function are easily determined analytically and the above integral may be determined in closed form. Numerically, we can only calculate these coefficients for a specific value of  $k_x$ .

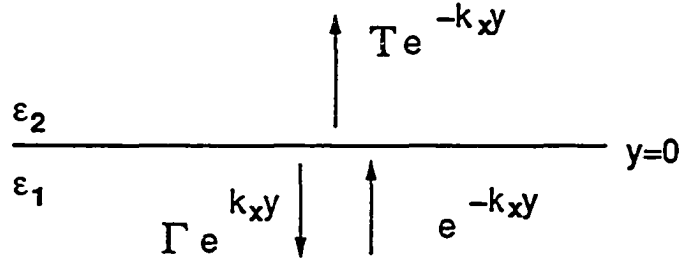


Figure 2.5: Single Dielectric Boundary Between the Source and Observation Points

Evaluation of the integral in this manner is not practical. Instead, let us assume that for large  $k_x$ , we have an asymptotic approximation  $\tilde{G}_\infty$  for  $\tilde{G}$ . Hence

$$G(\mathbf{r}|\mathbf{r}') = \frac{1}{\pi} \left\{ \int_0^{k_T} \tilde{G} \cos[k_x(x-x')] dk_x + \int_{k_T}^{\infty} \tilde{G}_\infty \cos[k_x(x-x')] dk_x \right\} \quad (2.66)$$

Where  $k_T$  is a value of  $k_x$  sufficiently large that the approximation  $\tilde{G}(k_T, y|y') \simeq \tilde{G}_\infty(k_T, y|y')$  is justified [2].

In order to construct the asymptotic approximation  $\tilde{G}_\infty$ , recall the following differential equation and corresponding boundary conditions in the spectral domain.

$$\frac{\partial^2 \tilde{G}}{\partial^2 y} - k_x^2 \tilde{G} = 0$$

$$\tilde{G}_i(d_i) = \tilde{G}_{i+1}(d_i)$$

$$\epsilon_{r,i} \frac{\partial \tilde{G}_i}{\partial y} \Big|_{d_i} = \epsilon_{r,i} \frac{\partial \tilde{G}_{i+1}}{\partial y} \Big|_{d_i} \quad (2.67)$$

Consider an arbitrary dielectric boundary, located somewhere between the source and observation points, where an attenuated wave is incident. Since at this

point, we are only interested in the transmission and reflection of the wave, we will place the boundary at  $y = 0$ . Furthermore, let us take the incoming wave to have a magnitude of 1 and the reflected and transmitted waves to magnitudes of  $\Gamma$  and  $T$ , respectively. Applying boundary conditions at  $y = 0$ , we obtain

$$\Gamma + 1 = T \quad (2.68)$$

$$-\epsilon_{r,2}T - \epsilon_{r,1}(\Gamma - 1) = 0 \quad (2.69)$$

From which we obtain the following transmission and reflection coefficients.

$$T = \frac{2\epsilon_{r,1}}{\epsilon_{r,1} + \epsilon_{r,2}} \quad (2.70)$$

$$\Gamma = \frac{\epsilon_{r,1} - \epsilon_{r,2}}{\epsilon_{r,1} + \epsilon_{r,2}} \quad (2.71)$$

For multiple dielectric boundaries between the source and observation points, the cascaded transmission line coefficient is

$$T = \prod_{i=k+1}^m \frac{2\epsilon_{r,i}}{\epsilon_{r,i} + \epsilon_{r,i+1}} \quad (2.72)$$

This is exactly as expected since the differential equation (2.67) is of the same form as that for the voltage along a multi-section transmission line [12]. Therefore, the solution of  $\tilde{G}$  may be thought of as the superposition of the direct wave and all multiply reflected waves. Each of these waves may be written as an amplitude multiplied by an attenuating factor  $e^{-k_x l}$ , where  $l$  is the total distance traveled by the wave.

In our asymptotic approximation of the spectral domain Green's function, only the slowest decaying exponentials in  $k_x$  will be retained. These correspond to those which travel the shortest distance  $l$  between the source and observation points. The four waves which will be retained in the asymptotic expression are shown in Figure 2.6. The accuracy and the necessity of the four wave approximation will be discussed in the next section.

Let us now develop an expression for the direct wave, which we will denote as  $\tilde{G}_\infty^{(1)}$ . First, we must determine the magnitude of the wave at the source location. For this, we will consider only outward directed waves at the boundary  $d_k$ .

Applying boundary conditions, we write

$$A_k e^{k_x d_k} = B_{k+1} e^{-k_x d_k} \quad (2.73)$$

$$-\epsilon_{r,k+1} B_{k+1} e^{-k_x d_k} - \epsilon_{r,k} A_k e^{k_x d_k} = -\frac{1}{k_x \epsilon_0} \quad (2.74)$$

Substituting (2.73) into (2.74), we obtain the magnitude of the upper wave

$$B_{k+1} = \frac{1}{k_x \epsilon_0 (\epsilon_{r,k} + \epsilon_{r,k+1})} e^{k_x d_k} \quad (2.75)$$

Therefore, at the observation point  $y$ , the expression for the direct wave is

$$\begin{aligned} \tilde{G}_\infty^{(1)}(k_x, y|y') &= T B_{k+1} e^{-k_x y} \\ &= \frac{1}{2k_x \epsilon_0 \epsilon_{r,k}} \prod_{i=k}^m \frac{2\epsilon_{r,i}}{\epsilon_{r,i} + \epsilon_{r,i+1}} e^{-k_x (y - d_k)} \end{aligned} \quad (2.76)$$

Similarly, the three reflected waves may be written as an amplitude multiplied by an attenuating factor  $e^{-k_x l}$ . These are



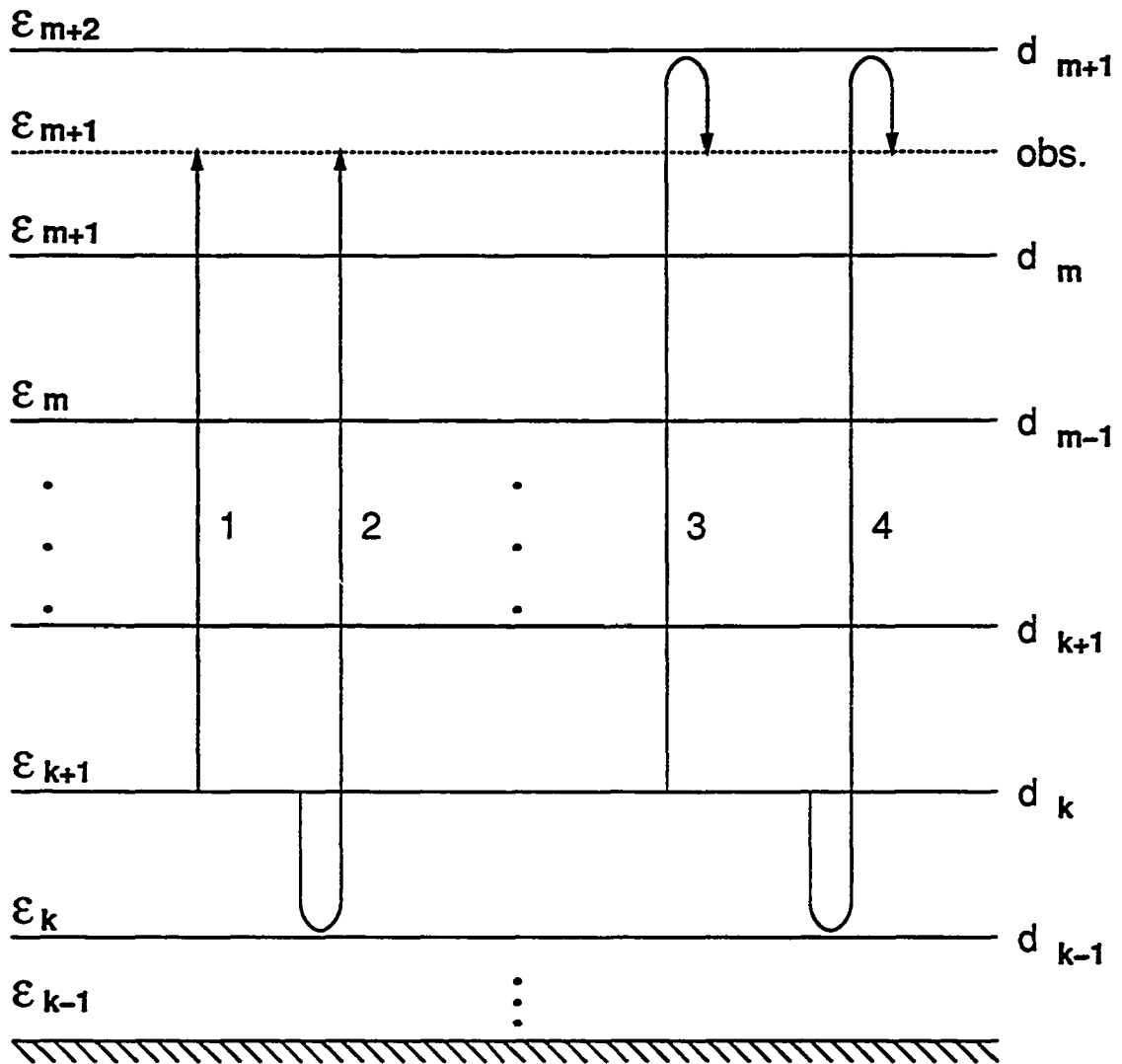
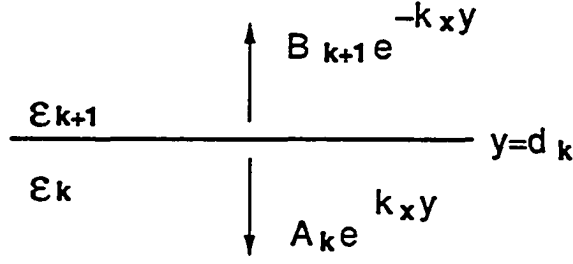


Figure 2.6: Four Slowest Decaying Attenuated Waves

Figure 2.7: Outward Directed waves Emanating from the Source at  $d_k$ 

$$\tilde{G}_{\infty}^{(2)} = \left( \frac{\epsilon_{r,k} - \epsilon_{r,k-1}}{\epsilon_{r,k} + \epsilon_{r,k-1}} \right) \frac{1}{2k_x \epsilon_0 \epsilon_{r,k}} \prod_{i=k}^m \frac{2\epsilon_{r,i}}{\epsilon_{r,i} + \epsilon_{r,i+1}} e^{-k_x(y-d_k+2(d_k-d_{k-1}))} \quad (2.77)$$

$$\tilde{G}_{\infty}^{(3)} = \left( \frac{\epsilon_{r,m+1} - \epsilon_{r,m+2}}{\epsilon_{r,m+1} + \epsilon_{r,m+2}} \right) \frac{1}{2k_x \epsilon_0 \epsilon_{r,k}} \prod_{i=k}^m \frac{2\epsilon_{r,i}}{\epsilon_{r,i} + \epsilon_{r,i+1}} e^{-k_x(y-d_k+2(d_{m+1}-y))} \quad (2.78)$$

$$\begin{aligned} \tilde{G}_{\infty}^{(4)} &= \left( \frac{\epsilon_{r,k} - \epsilon_{r,k-1}}{\epsilon_{r,k} + \epsilon_{r,k-1}} \right) \left( \frac{\epsilon_{r,m+1} - \epsilon_{r,m+2}}{\epsilon_{r,m+1} + \epsilon_{r,m+2}} \right) \frac{1}{2k_x \epsilon_0 \epsilon_{r,k}} \prod_{i=k}^m \frac{2\epsilon_{r,i}}{\epsilon_{r,i} + \epsilon_{r,i+1}} \\ &\times e^{-k_x(y-d_k+2(d_k-d_{k-1})2(d_{m+1}-y))} \end{aligned} \quad (2.79)$$

Neglecting all other reflected waves, the asymptotic approximation  $\tilde{G}_{\infty}$  may be written in the following compact form.

$$\tilde{G}_{\infty} = \sum_{i=1}^4 \tilde{G}_{\infty}^{(i)} = \sum_{i=1}^4 \frac{c_i}{k_x} e^{-k_x Y_i} \quad (2.80)$$

where

$$c_1 = \frac{1}{2\epsilon_0 \epsilon_{r,k}} \prod_{i=k}^m \frac{2\epsilon_{r,i}}{\epsilon_{r,i} + \epsilon_{r,i+1}} \quad (2.81)$$

$$c_2 = c_1 \left( \frac{\epsilon_{r,k} - \epsilon_{r,k-1}}{\epsilon_{r,k} + \epsilon_{r,k-1}} \right) \quad (2.82)$$

$$c_3 = c_1 \left( \frac{\epsilon_{r,m+1} - \epsilon_{r,m+2}}{\epsilon_{r,m+1} + \epsilon_{r,m+2}} \right) \quad (2.83)$$

$$c_4 = c_2 \left( \frac{\epsilon_{r,m+1} - \epsilon_{r,m+2}}{\epsilon_{r,m+1} + \epsilon_{r,m+2}} \right) \quad (2.84)$$

and

$$Y_1 = y - d_k \quad (2.85)$$

$$Y_2 = Y_1 + 2(d_k - d_{k-1}) \quad (2.86)$$

$$Y_3 = Y_1 + 2(d_{m+1} - y) \quad (2.87)$$

$$Y_4 = Y_2 + 2(d_{m+1} - y) \quad (2.88)$$

## 2.4 Numerical Comparison of the Spectral Domain Green's Functions

In the previous section, we developed the asymptotic approximation for the spectral domain Green's function. This approximation was constructed in terms of four attenuated waves with precisely specified pathlengths. In this section, we will discuss the validity of this approximation.

Consider the layered medium of Figure 2.8 for the purposes of comparing the two functions. This medium was selected because the asymptotic expression

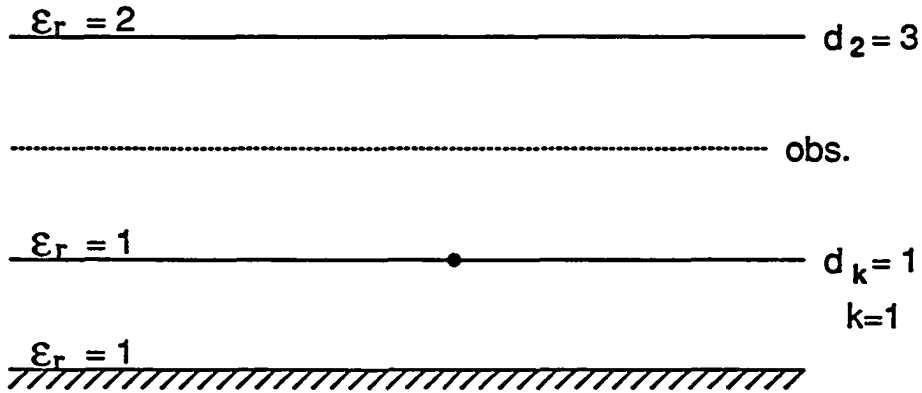


Figure 2.8: Layered medium used in the comparison of the spectral domain Green's function and its asymptotic approximation

at the observation point contains all four waves. We will compare the spectral domain Green's function to the asymptotic approximation and determine how the value of  $k_T$  depends on the number of waves taken in the approximation. Also, we will be examining the problems encountered when the layered dielectric medium contains one or more layers which are much thinner than the other layers.

The first comparison, shown in Figure 2.9, is of the spectral Green's function and the asymptotic approximation containing all four waves. Note that the coefficients of  $\tilde{G}$  used to generate these plots were determined numerically using the matrix method previously discussed. Here, we see that the asymptotic expression exactly corresponds to  $\tilde{G}$  after some value  $k_T$ . If we choose  $K_T$  as the value of  $k_x$  at which the relative difference between  $\tilde{G}$  and  $\tilde{G}_\infty$  is less than  $10^{-6}$ , then for Figure 2.9,  $k_T = 2.11$ . If the number of waves in  $\tilde{G}_\infty$  is reduced, the value of  $k_T$  increases. This can be seen in Figures 2.10-2.12 where the number of terms in  $\tilde{G}_\infty$  goes from three to one. In these examples, the values of  $k_T$  are 3.15, 6.35 and 7.01, respectively. Since the value of  $M$ , the number of subintervals into which  $(0, k_T)$  is subdivided, is determined depending on the value of  $k_T$ , the computation time for integrating  $\tilde{G}$  over  $(0, k_T)$  increases. It will become apparent in the next chapter that this integration, along with the procedure for computing the coefficients  $A_{m+1}$

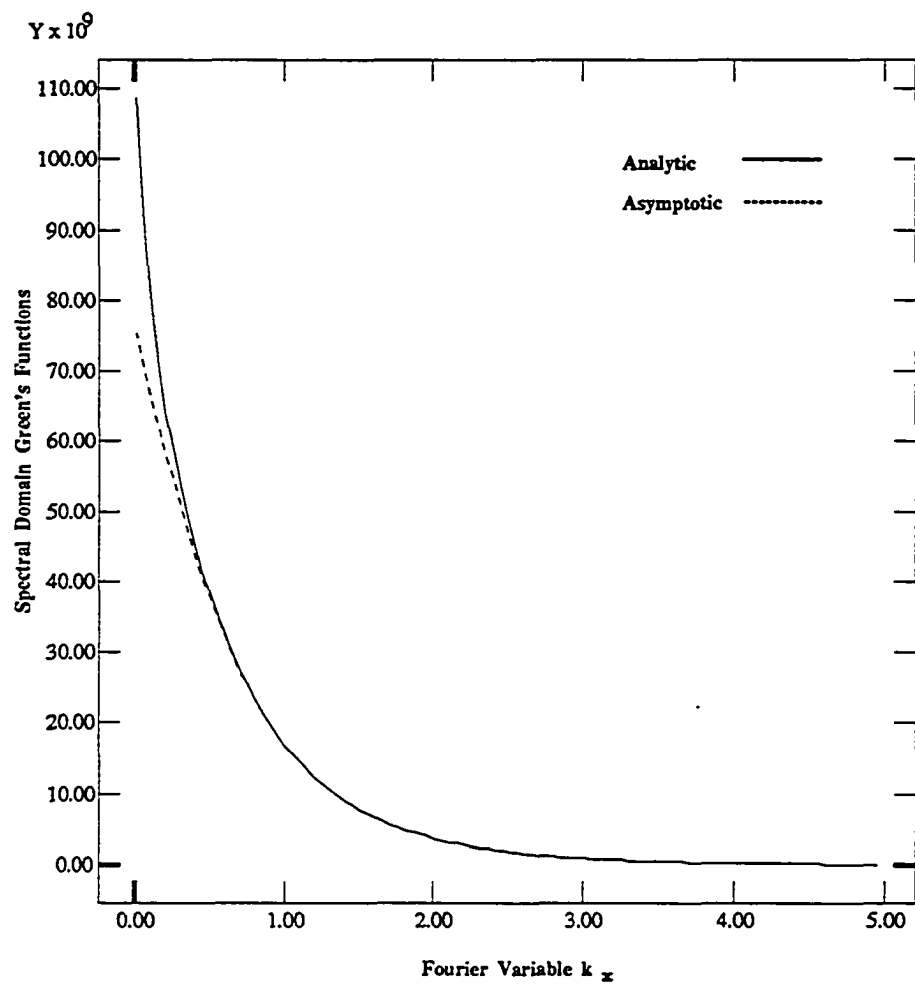


Figure 2.9: Spectral domain Green's function compared with the four wave asymptotic approximation

and  $B_{m+1}$  requires more computation time than any other aspect of the method.

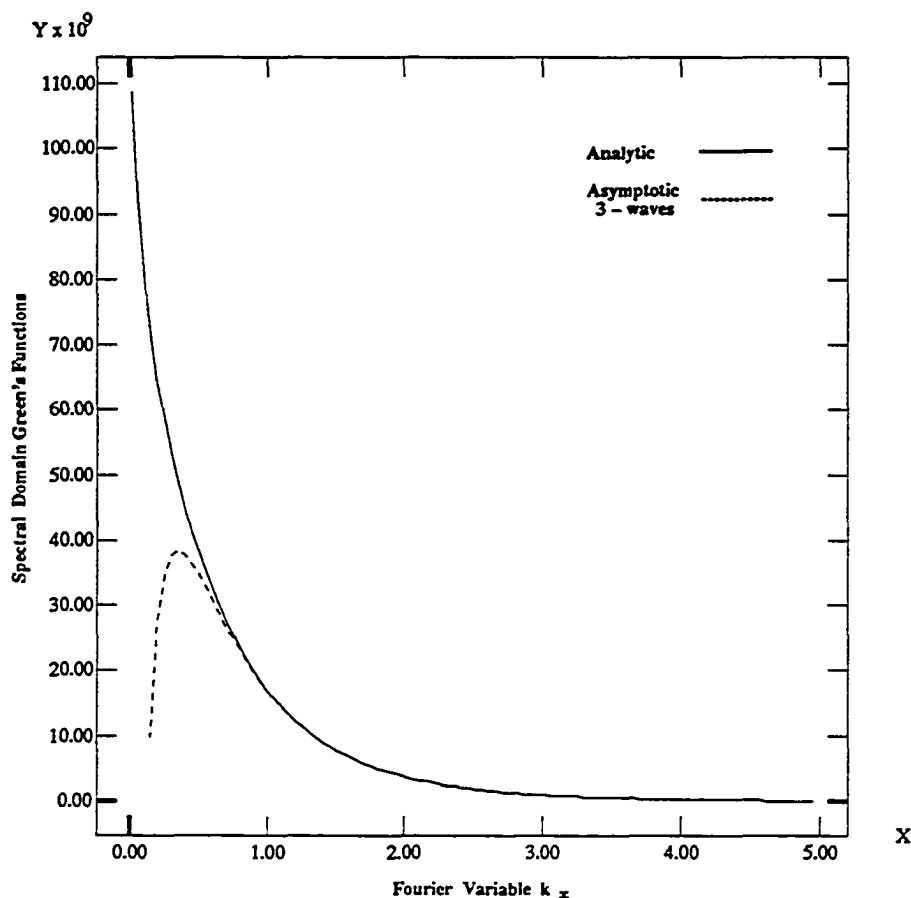


Figure 2.10: Spectral domain Green's function compared with the three wave asymptotic approximation

Scaling of the  $(x,y)$  coordinates of the geometry also has a significant effect on the value of  $k_T$ . To show this, again consider the layered dielectric geometry of Figure (2.8). If we multiply all coordinates by a factor of 10, the resulting plots of Figure 2.13 shows that much smaller value,  $k_T = 0.21$ . However, if we divide all coordinated by the same factor of 10, we obtain the opposite result. Figure (2.14) shows that  $k_T$  has increased, to 21.1. this suggests that a scaling routine can significantly reduce  $k_T$  and hence the computation time involved.

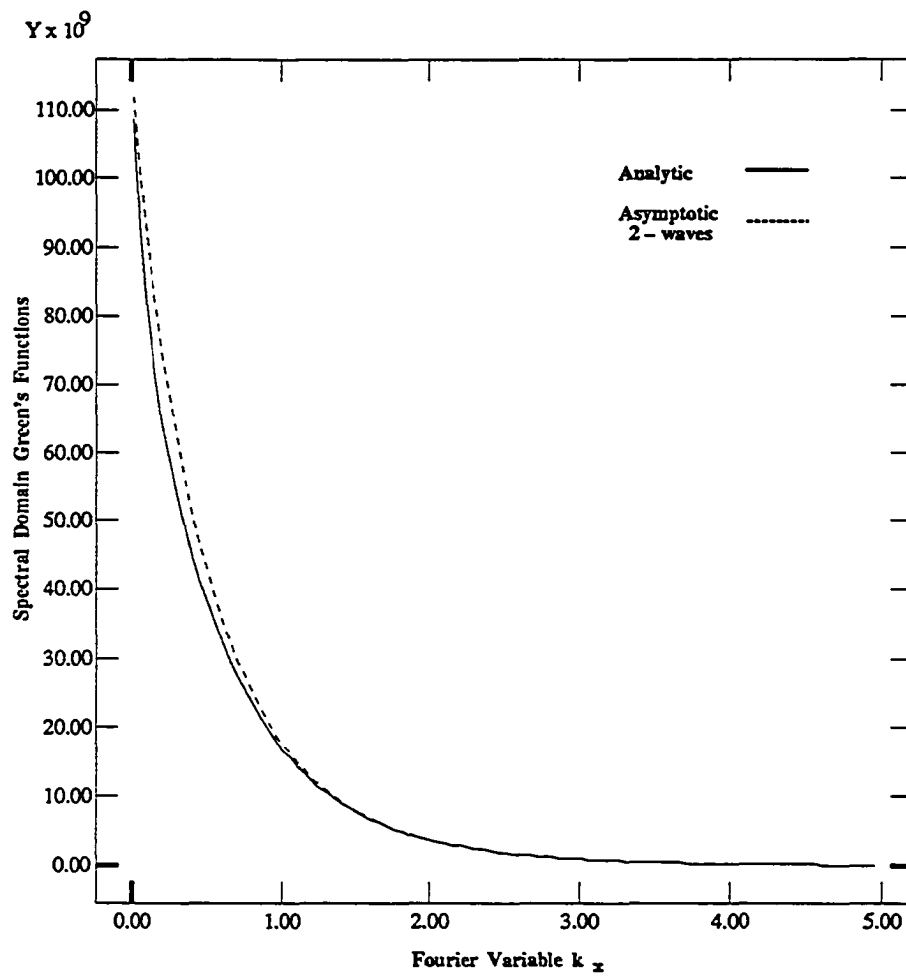


Figure 2.11: Spectral domain Green's function compared with the two wave asymptotic approximation

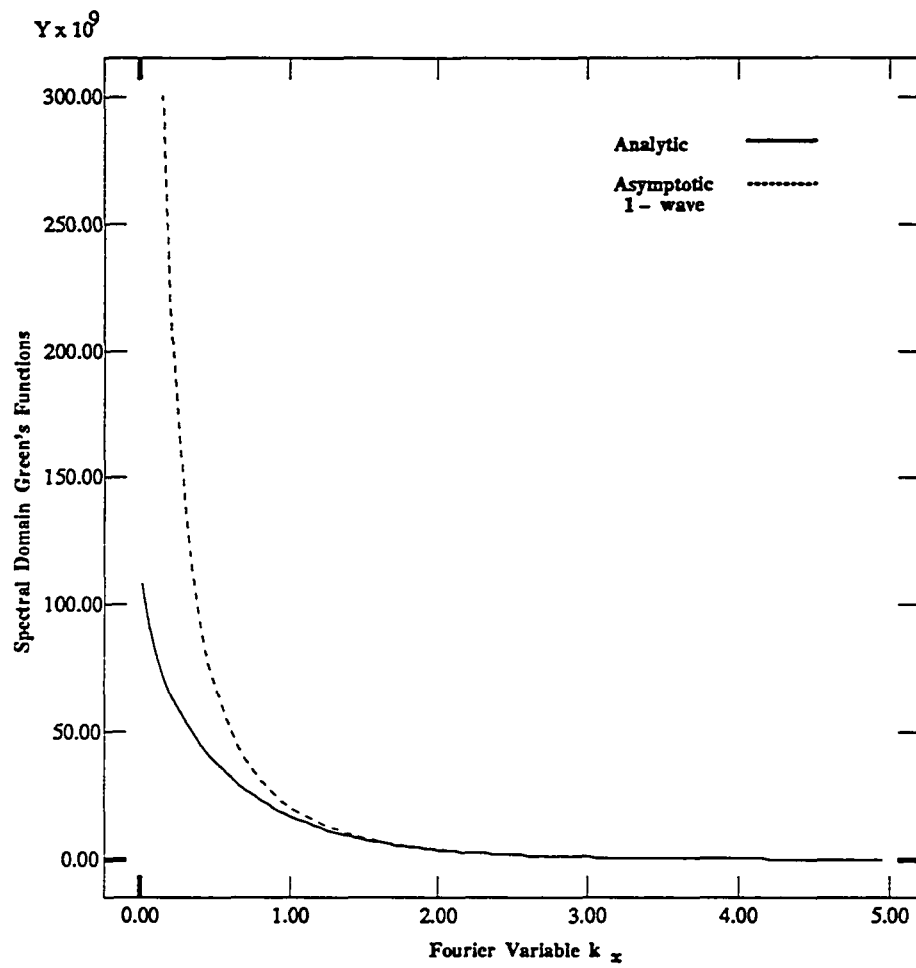


Figure 2.12: Spectral domain Green's function compared with a single wave asymptotic approximation



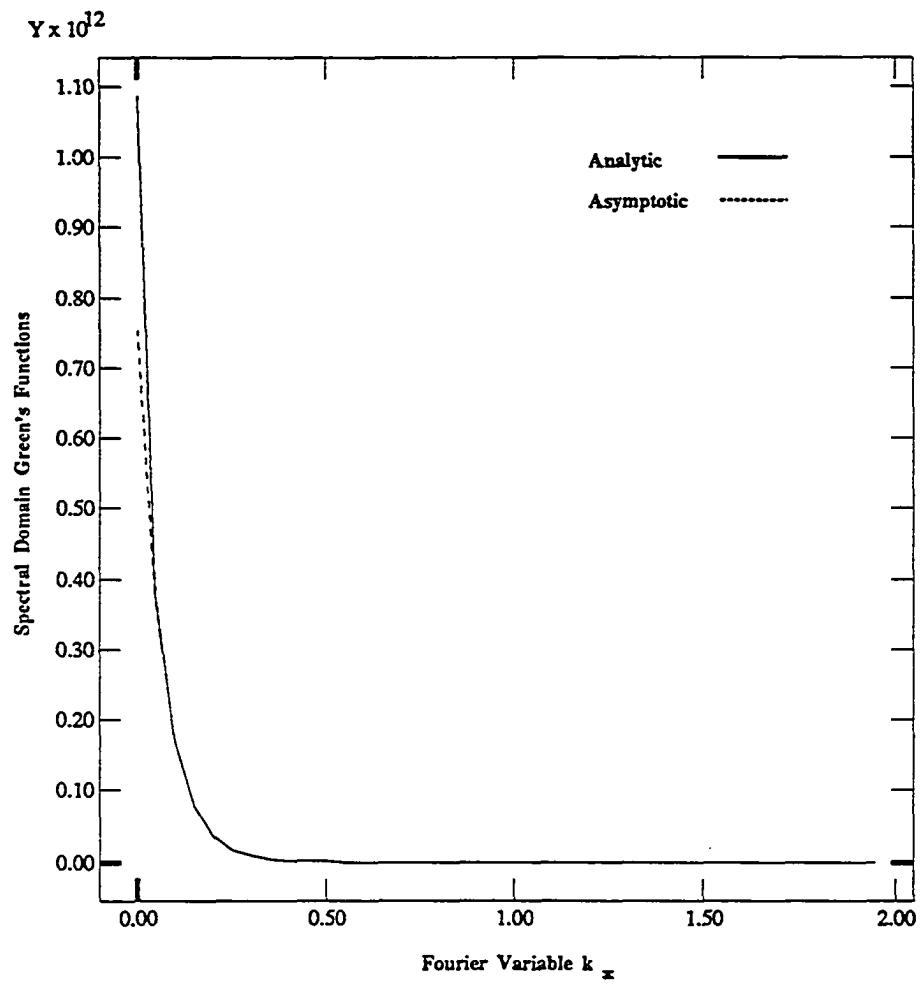


Figure 2.13: Effect of positive coordinate scaling on  $k_T$

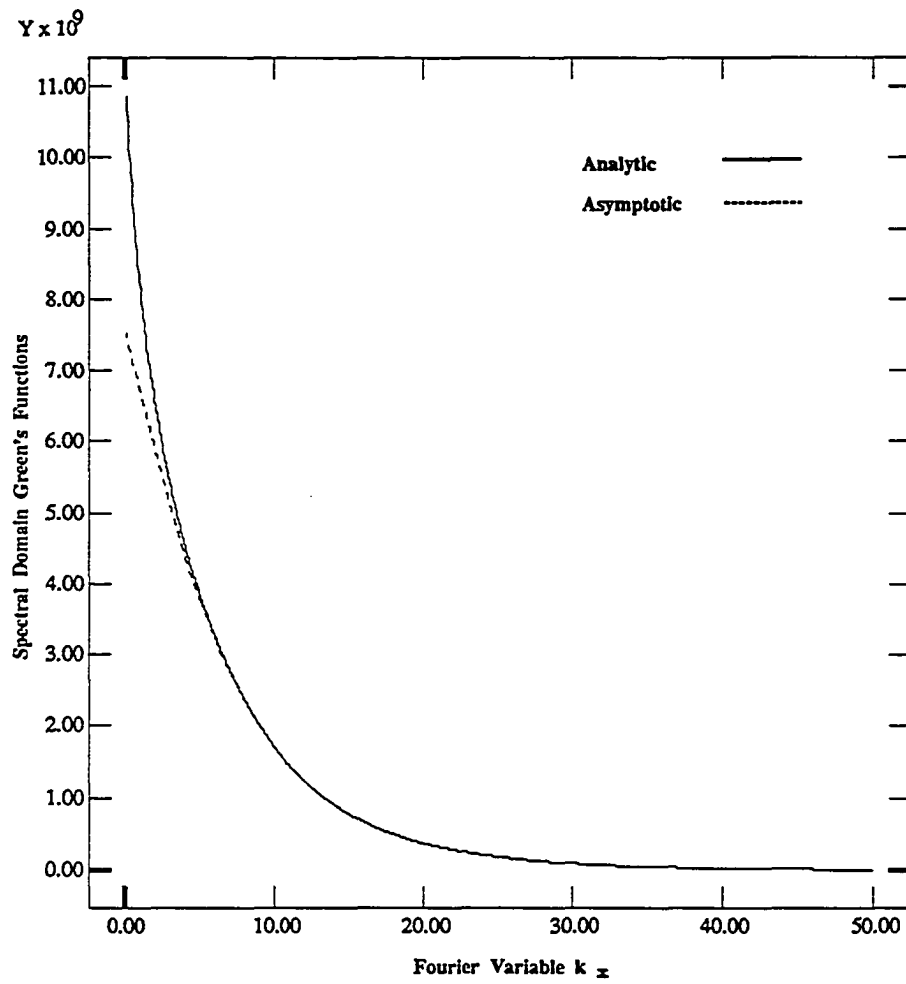


Figure 2.14: Effect of negative coordinate scaling on  $k_T$

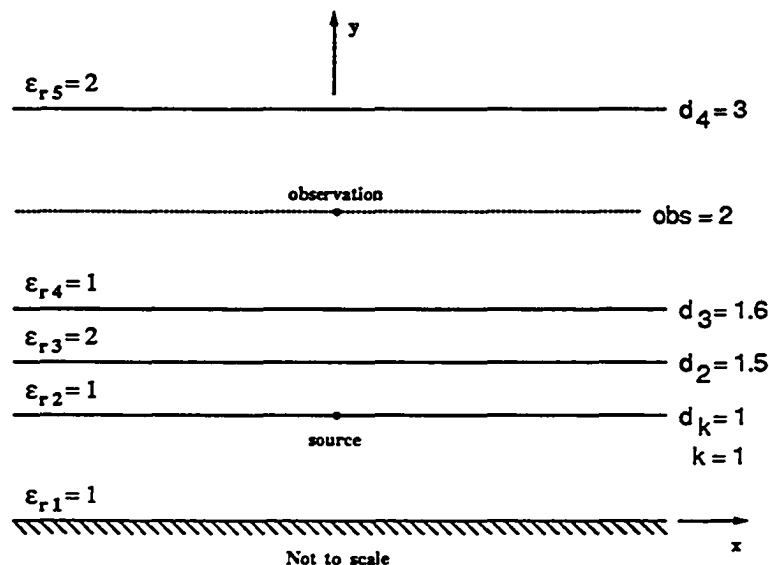


Figure 2.15: Layered medium with a thin layer between the source and observation points

Let us now consider how the asymptotic approximation will suffer when very thin layers are included in the layered medium. For this, consider the medium of Figure 2.15. Here, a thin layer has been inserted into the previous medium. In this case, the asymptotic approximation  $\tilde{G}_\infty$  no longer contains the attenuated waves with the shortest pathlengths. In fact, aside from the direct wave, the waves with the shortest pathlengths are those with multiple reflections within the thin layer. These are shown in figure 2.16. The comparison of the spectral domain Green's function and the two asymptotic approximations are shown in Figure 2.17. Here, it looks as if the standard asymptotic expression more closely and more quickly approximates the analytical expression compared with the modified asymptotic approximation. Actually, the modified asymptotic approximation produces a much lower value of  $k_T$  than the standard approximation. The modified approximation yields  $k_T = 12.75$  compared to  $k_T = 58.05$  for the standard approximation. This

implies that the asymptotic approximation based on the four waves of Figure 2.6 is not the best approximation to  $\tilde{G}$  when the multilayered medium contains layers that are much thinner than the others. In fact, since  $\tilde{G}$  essentially decays to zero at  $k_x = 23.8$ , the four wave approximation of Figure 2.6 may be considered unnecessary in this case.

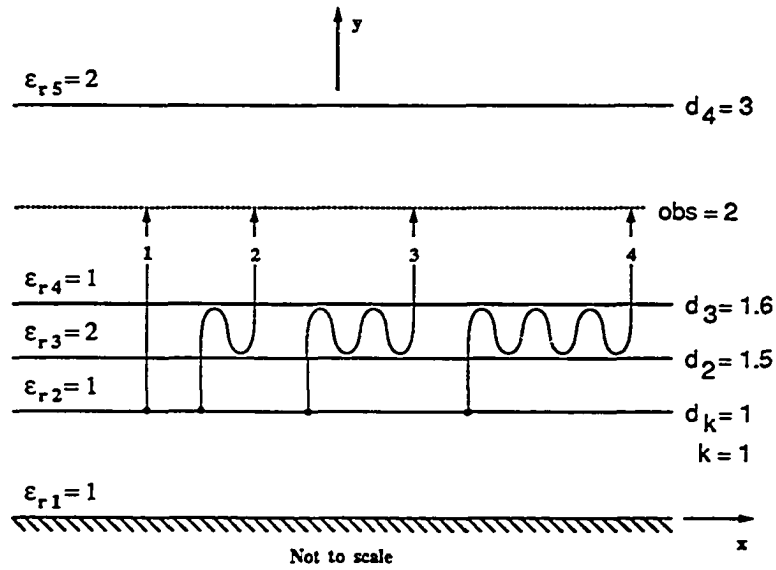


Figure 2.16: Four attenuated waves with the shortest pathlengths

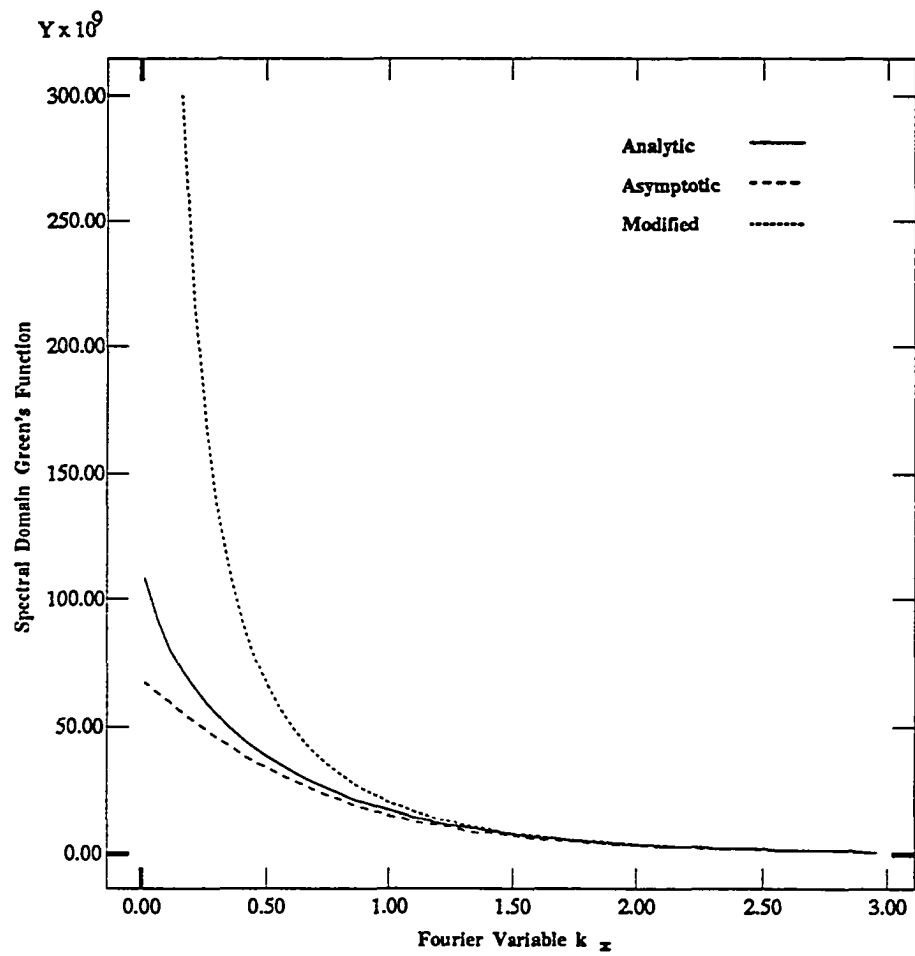


Figure 2.17: Comparison between asymptotic approximations constructed from different attenuated waves

## 2.5 Space Domain Green's Function

The space domain Green's function for the layered medium is obtained by taking the inverse Fourier cosine transform of the spectral domain Green's function. As stated in the previous section, the integration over  $[0, \infty]$  is broken into two parts. Let us now substitute  $\tilde{G}$  and  $\tilde{G}_\infty$  into equation (2.66).

$$\begin{aligned}
 G(\mathbf{r}|\mathbf{r}') &= \frac{1}{\pi} \left\{ \int_0^{k_T} (A_{m+1}e^{k_x y} + B_{m+1}e^{-k_x y}) \cos[k_x(x-x')] dk_x \right. \\
 &\quad \left. + \sum_{i=1}^4 c_i \int_{k_T}^{\infty} \frac{1}{k_x} e^{-k_x Y_i} \cos[k_x(x-x')] dk_x \right\} \\
 &= G_{k_T} + G_\infty
 \end{aligned} \tag{2.89}$$

The constant  $k_T$  is found by computation and comparison for every case as the value of  $k_x$  such that the relative difference between the spectral domain Green's function and its asymptotic approximation is less than  $10^{-6}$ .

Evaluation of  $G_{k_T}$  at the observation point is performed numerically using Gaussian quadrature. The coefficients  $A_{m+1}$  and  $B_{m+1}$  are determined by the matrix procedure previously outlined for a specific value of  $k_x$ . In solving for  $G_{k_T}$ , we simply break up the integral over  $[0, k_T]$  into  $M$  subintervals.

$$G_{k_T}(k_x, y|y') = \frac{1}{\pi} \sum_{j=1}^M \int_{(j-1)k_T/M}^{jk_T/M} (A_{m+1}e^{k_x y} + B_{m+1}e^{-k_x y}) \cos[k_x(x-x')] dk_x \tag{2.90}$$

Finally, Gaussian quadrature is employed to evaluate the sum of integrals.

In evaluating  $G_\infty$ , we must first recognize that the integral over  $[k_T, \infty]$  has the following closed form solution, for  $Y_1 \neq 0$

$$\int_{k_T}^{\infty} \frac{1}{k_x} e^{-k_x Y_i} \cos[k_x(x - x')] dk_x = \text{Re}\{E_1(z)\} \quad (2.91)$$

where  $z = k_T Y_i + j k_T(x - x')$ , and  $\text{Re}\{E_1(z)\}$  is the real part of the exponential integral function the numerical evaluation of which is well documented [14]. If we insert (2.91) into  $G_{\infty}$ , we obtain

$$G_{\infty} = \frac{1}{\pi} \sum_{i=1}^4 c_i \text{Re}\{E_1(z)\} \quad (2.92)$$

If now  $Y_1 = 0$ , equation (2.91) becomes

$$\int_{k_T}^{\infty} \frac{1}{k_x} \cos[k_x(x - x')] dk_x = -Ci(k_T|x - x'|) \quad (2.93)$$

where  $Ci(k_T|x - x'|)$  is the cosine integral function, which may also be evaluated numerically [14]. Both the exponential integral and cosine integral functions and there numerical approximations are discussed in Appendix A. Our solution for  $G_{\infty}$  for the case where  $Y_1 = 0$  now becomes

$$G_{\infty} = -\frac{c_1}{\pi} Ci(k_T|x - x'|) + \frac{1}{\pi} \sum_{i=2}^4 c_i \text{Re}\{E_1(z)\} \quad (2.94)$$

Finally, note that the cosine integral is singular at  $x = x'$ . When integrating the Green's function over an element which includes the point  $x = x'$ , a special quadrature formula is used. This formula places quadrature points more closely around the singularity, improving the accuracy of the numerical integration [11]. This quadrature formula is presented in Appendix B.

## CHAPTER 3

### Numerical Solution of the Integral Equation

In the previous chapter, the space domain Green's function was obtained for the layered dielectric medium. Once the Green's function is known everywhere, we may proceed with the formulation of the integral equation for the total charge distribution on the surfaces of the conductors and the non-planar dielectric boundaries for given potential boundary conditions. The integral equation will be solved numerically using the method of moments [1-3].

#### 3.1 Method of Moments solution for the Charge Distribution

There are two types of interfaces to consider. These are conductor-dielectric and non-planar dielectric-dielectric interfaces. The geometry, along with the discretized interfaces indicated by the dashed lines, is shown in Figure 3.1. We are interested in solving (2.8) for the case where the  $i^{th}$  conductor is set at a potential of 1 volt, while all others are grounded. The integral of the free charge density over the  $i^{th}$  conductor boundary due to the  $j^{th}$  conductor charged to 1 volt then becomes the  $C_{ij}$  element of the capacitance matrix.

The potential at a point  $\mathbf{r}$  on the  $i^{th}$  interface due to the total charge on conductor surfaces and dielectric-dielectric interfaces is given by



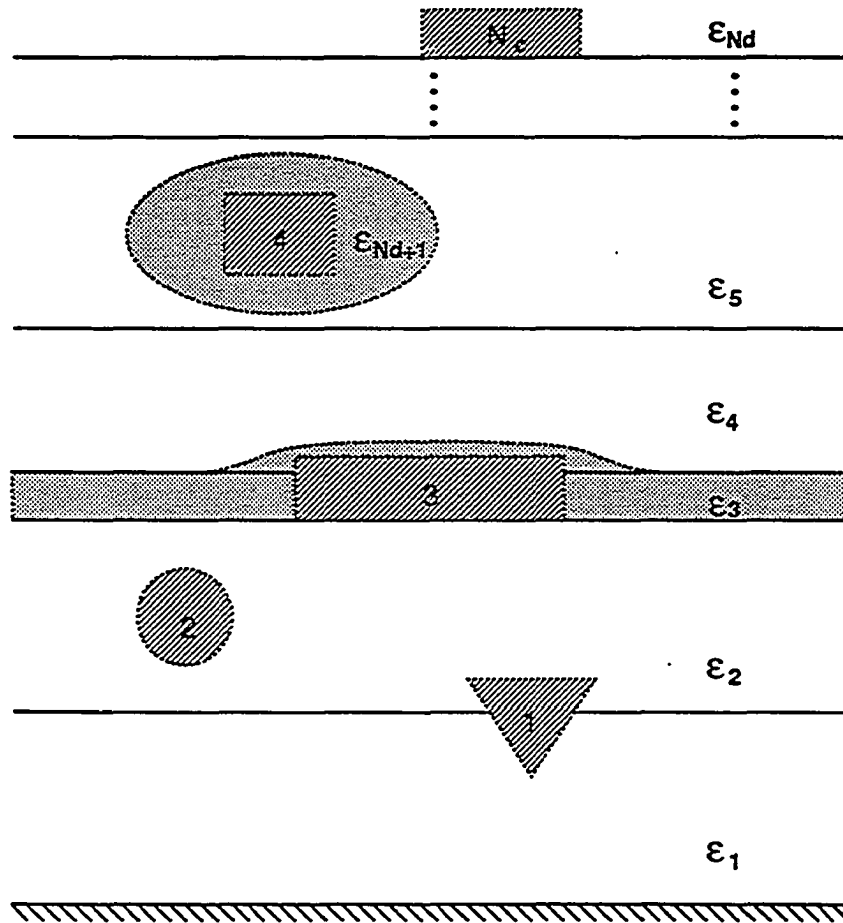


Figure 3.1: Cross Section of General Discretized Geometry

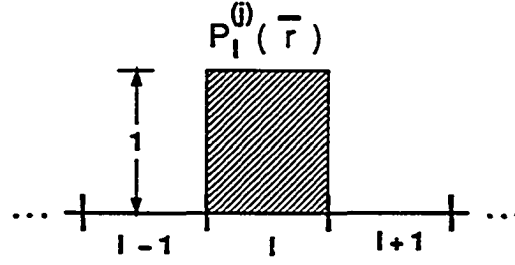


Figure 3.2: Unit Pulse Function

$$V_i = \sum_{j=1}^N \int_{C_j} \sigma_{Tj}(\mathbf{r}') G(\mathbf{r}|\mathbf{r}') dl' \quad (3.1)$$

where  $\sigma_{Tj}(\mathbf{r}')$  is the total surface charge density and  $N$  is the total number of interfaces, of which  $N_c$  are conductor-dielectric interfaces and  $N - N_c$  are dielectric-dielectric interfaces. The charge distribution on the  $j^{th}$  interface may be approximated in a piecewise constant manner as

$$\sigma(\mathbf{r}') = \sum_{l=1}^{M_j} \sigma_l^{(j)} P_l^{(j)}(\mathbf{r}') \quad , \quad i = 1, 2, \dots, N_c \quad (3.2)$$

where  $M_j$  is the number of segments on the  $j^{th}$  interface and  $P_l^{(j)}(\mathbf{r}')$  are unit pulse functions defined to be 1 over the  $l^{th}$  segment of the  $j^{th}$  interface and zero everywhere else. Since the unit pulse function is 1 over the entire segment,  $\sigma_l^j$  represents a constant approximation of the charge density on the  $l^{th}$  segment of the  $j^{th}$  interface.

Substituting (3.2) into (3.1), we obtain

$$V_i = \sum_{j=1}^N \int_{C_j} \left\{ \sum_{l=1}^{M_j} \sigma_l^{(j)} P_l^{(j)}(\mathbf{r}') \right\} G(\mathbf{r}|\mathbf{r}') dl' \quad (3.3)$$

We can rewrite this as

$$V_i = \sum_{j=1}^N \sum_{l=1}^{M_j} \sigma_l^{(j)} \int_{C_j} P_l^{(j)}(\mathbf{r}') G(\mathbf{r}|\mathbf{r}') dl' \quad (3.4)$$

However,  $P_l^{(j)}(\mathbf{r}')$  is only nonzero over the  $l^{th}$  segment of the  $j^{th}$  interface,  $\Delta C_l^{(j)}$ , so

$$V_i = \sum_{j=1}^N \sum_{l=1}^{M_j} \sigma_l^{(j)} \int_{\Delta C_l^{(j)}} G(\mathbf{r}|\mathbf{r}') dl' \quad (3.5)$$

Since  $G(\mathbf{r}|\mathbf{r}')$  is known, the integral over  $\Delta C_l^{(j)}$  is also known. Assuming that  $\mathbf{r}$  is the position vector for the midpoint of the  $k^{th}$  segment of the  $i^{th}$  conductor, let us denote this integral as

$$\begin{aligned} Z_{k_i l_j} &= \int_{\Delta C_l^{(j)}} G(\mathbf{r}|\mathbf{r}') dl' \\ &= \int_{\Delta C_l^{(j)}} \{G_{k_T}(\mathbf{r}|\mathbf{r}') + G_{\infty}(\mathbf{r}|\mathbf{r}')\} dl' \end{aligned} \quad (3.6)$$

So that the potential may be written in the following convenient form

$$V_i = \sum_{j=1}^N \sum_{l=1}^{M_j} \sigma_l^{(j)} Z_{k_i l_j} \quad (3.7)$$

The indices of  $Z_{k_i l_j}$  represent the value of the integral of the Green's function at the midpoint of the  $k^{th}$  segment of the  $i^{th}$  interface due to the  $l^{th}$  segment of the  $j^{th}$  conductor.

Recall that the general problem consists of  $N_C$  conductor-dielectric interfaces and  $N - N_C$  dielectric-dielectric interfaces. Furthermore, the  $i^{th}$  interface is

subdivided into  $M_i$  subintervals. Equation (3.7) is employed for the point-matching procedure used in the method of moments for the numerical approximation of the integral equation. By enforcing (3.7) at the center of each segment of the conductor contours we obtain a system of  $\sum_{i=1}^{N_c} M_i$  equations for a total of  $\sum_{i=1}^N M_i$  unknowns. If there are no non-planar dielectric regions present,  $N = N_C$  and the system is solvable. However when non-planar dielectric interfaces are present, the system is underdetermined. In this case another set of  $\sum_{i=N_C+1}^N M_i$  equations is required to determine the system. These equations are associated with the polarization charge distribution along the dielectric-dielectric interfaces and are obtained by enforcing continuity of the potential and the normal component of the electric flux across these interfaces.

The electric field  $\mathbf{E}(\mathbf{r})$  is expressed in terms of the potential by

$$\mathbf{E}(\mathbf{r}) = -\nabla\phi(\mathbf{r}) \quad (3.8)$$

Substituting (3.1) into the above expression, we have

$$\mathbf{E}(\mathbf{r}) = -\sum_{j=1}^N \nabla \int_{C_j} \sigma_{Tj}(\mathbf{r}') G(\mathbf{r}|\mathbf{r}') dl' \quad (3.9)$$

Bringing the  $\nabla$  operator inside the integral, we have

$$\mathbf{E}(\mathbf{r}) = -\sum_{j=1}^N \int_{C_j} \sigma_{Tj}(\mathbf{r}') \nabla G(\mathbf{r}|\mathbf{r}') dl' \quad (3.10)$$

So we must derive an expression for  $\nabla G(\mathbf{r}|\mathbf{r}')$ . It is

$$\nabla G(\mathbf{r}|\mathbf{r}') = \left( \hat{x} \frac{\partial}{\partial x} + \hat{y} \frac{\partial}{\partial y} \right) G(\mathbf{r}|\mathbf{r}')$$

$$\begin{aligned}
&= \hat{x} \frac{-1}{\pi} \int_0^\infty k_x \tilde{G} \sin[k_x(x - x')] dk_x \\
&+ \hat{y} \frac{1}{\pi} \int_0^\infty \frac{d\tilde{G}}{dy} \cos[k_x(x - x')] dk_x \quad (3.11)
\end{aligned}$$

At this point, we must justify taking the derivative of the asymptotic approximation in (3.11). For this, let us consider the simple layered medium of Figure 3.3. For this case, we will compare the derivative of the asymptotic approximation with the derivative of the analytical approximation as functions of  $k_x$ . Recall that comparisons of the Green's function and the asymptotic approximation were made previously in chapter 2. The comparative plot of the derivatives of  $\tilde{G}$  and  $\tilde{G}_\infty$  is shown in figure 3.4, respectively.

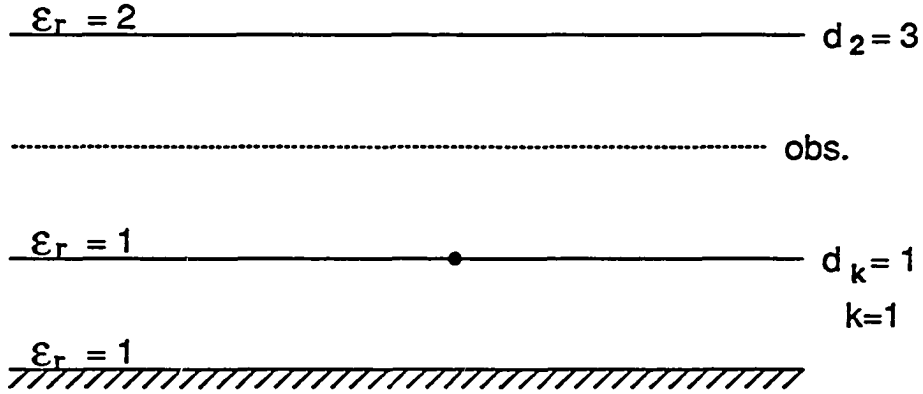


Figure 3.3: Layered geometry for analytic and asymptotic spectral domain Green's function comparisons

Substituting for the spectral domain Green's function  $\tilde{G}$  for a point  $\mathbf{r}$  in the  $(m + 1)^{th}$  interface into (3.11) yields

$$\nabla G(\mathbf{r}|\mathbf{r}') = - \hat{x} \frac{1}{\pi} \int_0^{k_T} k_x \left( A_{m+1} e^{k_x y} + B_{m+1} e^{-k_x y} \right) \sin[k_x(x - x')] dk_x$$

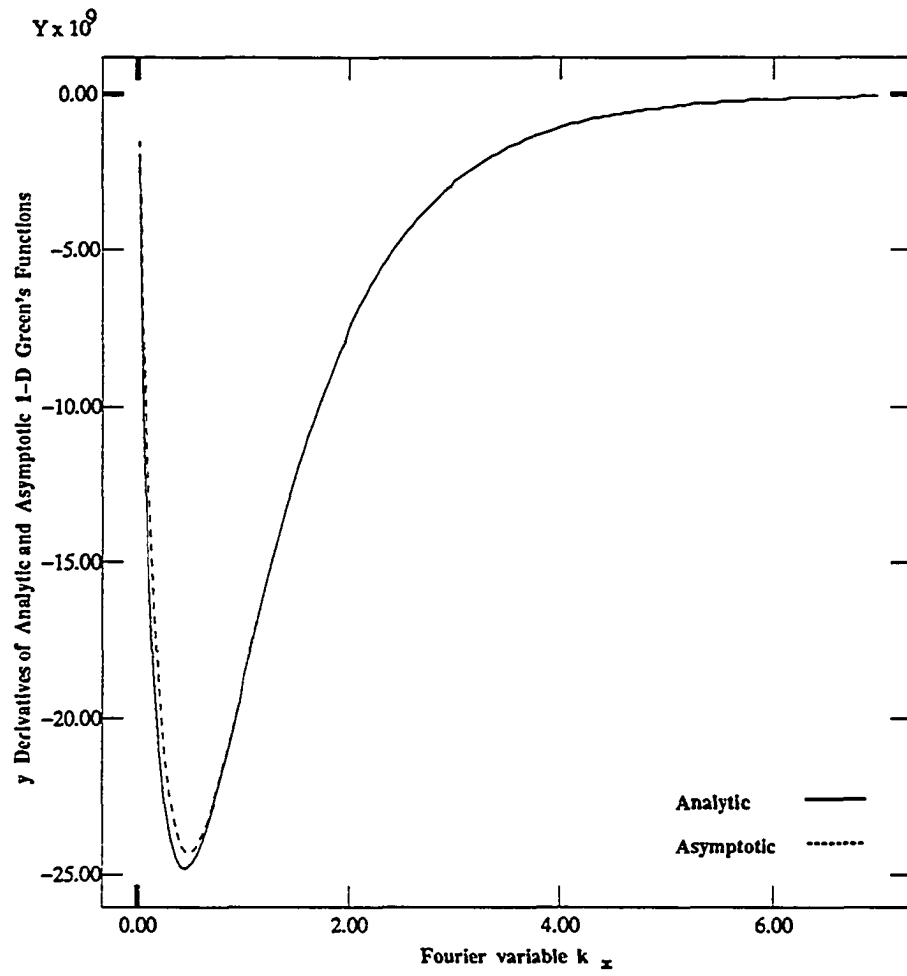


Figure 3.4: Comparison of the derivatives for the analytic and asymptotic spectral domain Green's functions

$$\begin{aligned}
& - \hat{x} \sum_{i=1}^4 \frac{c_i}{\pi} \int_{k_T}^{\infty} e^{-k_x Y_i} \sin[k_x(x-x')] dk_x \\
& + \hat{y} \frac{1}{\pi} \int_0^{k_T} k_x (A_{m+1} e^{k_x y} - B_{m+1} e^{-k_x y}) \cos[k_x(x-x')] dk_x \\
& + \hat{y} \sum_{i=1}^4 \mp \frac{c_i}{\pi} \int_{k_T}^{\infty} e^{-k_x Y_i} \cos[k_x(x-x')] dk_x \tag{3.12}
\end{aligned}$$

where the  $\mp$  sign of the fourth term is specifically  $-$  for  $i = 1, 2$  and  $+$  for  $i = 3, 4$ . This is due to the sign obtained from taking the derivative  $dY_i/dy$ . Since in the first and third terms  $A_{m+1}$  and  $B_{m+1}$  are in general only solvable numerically for a specific value of  $k_x$ , Gaussian quadrature is used to evaluate a sum of integrals over subsections of the interval  $(0, k_x)$  where  $A_{m+1}$  and  $B_{m+1}$  are taken to be constants calculated using the value of  $k_x$  at the quadrature points of each subinterval. On the other hand, the integrals over  $(T, \infty)$  are solvable analytically and are found in tables. Hence the final expression for  $\nabla G(\mathbf{r}|\mathbf{r}')$  becomes

$$\begin{aligned}
\nabla G(\mathbf{r}|\mathbf{r}') = & - \hat{x} \frac{1}{\pi} \int_0^{k_T} k_x (A_{m+1} e^{k_x y} + B_{m+1} e^{-k_x y}) \sin[k_x(x-x')] dk_x \\
& - \hat{x} \frac{1}{\pi} \sum_{i=1}^4 \frac{c_i e^{-k_T Y_i}}{(x-x')^2 + Y_i^2} \\
& \times \{Y_i \sin[k_T(x-x')] + (x-x') \cos[k_T(x-x')]\} \\
& + \hat{y} \frac{1}{\pi} \int_0^{k_T} k_x (A_{m+1} e^{k_x y} - B_{m+1} e^{-k_x y}) \cos[k_x(x-x')] dk_x \\
& + \hat{y} \frac{1}{\pi} \sum_{i=1}^4 \mp \frac{c_i e^{-k_T Y_i}}{(x-x')^2 + Y_i^2} \\
& \times \{Y_i \cos[k_T(x-x')] - (x-x') \sin[k_T(x-x')]\} \tag{3.13}
\end{aligned}$$

Notice that the second and fourth terms are singular when both  $x = x'$  and  $Y_1 = 0$ . This will occur when the observation point lies at the center of the source interval over which we are integrating. To evaluate these integrals, we need to extract the singularity and calculate the integral in the Cauchy principle value sense [5].

To complete the set of equations, we apply boundary conditions at the dielectric-dielectric interfaces. First, the normal component of the electric flux must be continuous across the dielectric-dielectric interfaces. Consider an arbitrary interface between two regions with dielectric constants  $\epsilon_1$  and  $\epsilon_2$ , with the normal vector  $\hat{n}$  pointing into the region of  $\epsilon_2$ . At this boundary, we write

$$\epsilon_1 \mathbf{E}_1(\mathbf{r}) \cdot \hat{n} = \epsilon_2 \mathbf{E}_2(\mathbf{r}) \cdot \hat{n} \quad (3.14)$$

By examining equations (3.10) and (3.11) we notice that in the limit as  $\mathbf{r} \rightarrow \mathbf{r}'$   $\mathbf{E}(\mathbf{r})$  involves the integration of  $\nabla G$  along  $C_j$ ,  $j = N_c + 1, N_c + 2, \dots, N$ , which includes the singular point  $\mathbf{r} = \mathbf{r}'$ . In order to extract this singularity, let us examine the singular nature of the Green's function. In an arbitrary medium such as ours, the Green's function may be written as the superposition of primary and secondary contributions, where the primary term is defined to be the potential at  $\mathbf{r}$  due to a line source at  $\mathbf{r}'$  in the absence of any medium interfaces.

$$G(\mathbf{r}|\mathbf{r}') = G^p(\mathbf{r}|\mathbf{r}') + G^s(\mathbf{r}|\mathbf{r}') \quad (3.15)$$

Although the secondary term involves the effects of dielectric interfaces and ground planes on the potential, it does not contain any singularities. Therefore the primary term, which is simply the free space Green's function in two dimensions, is the one responsible for the singular nature of the Green's function

$$G^p(\mathbf{r}|\mathbf{r}') = \frac{-1}{2\pi\epsilon_0} \ln |\mathbf{r} - \mathbf{r}'| \quad (3.16)$$



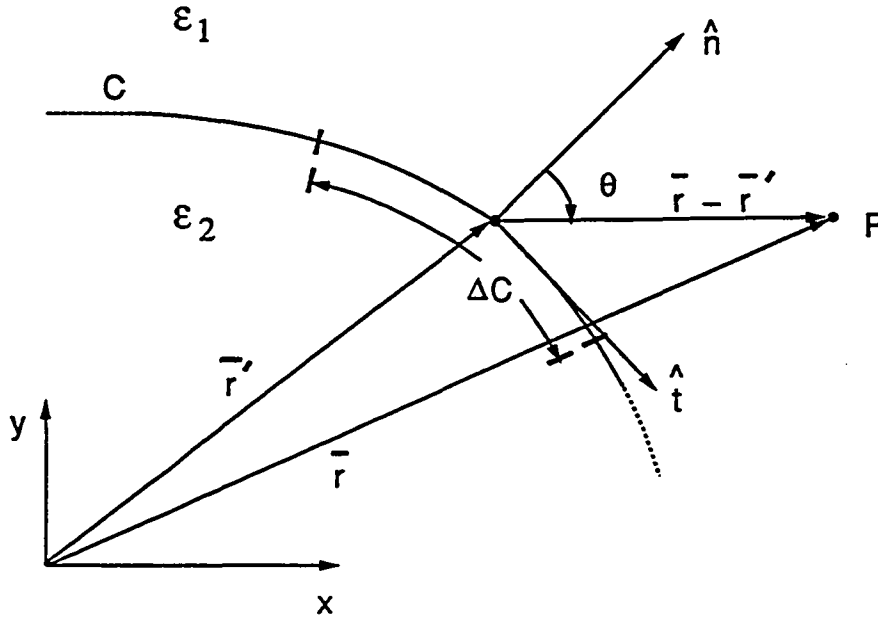


Figure 3.5: Arbitrary Dielectric Interface

Thus, the singularity of  $\nabla G(\mathbf{r}|\mathbf{r}')$  is solely due to  $\nabla G^p$ , which is

$$\nabla G^p(\mathbf{r}|\mathbf{r}') = \frac{-1}{2\pi\epsilon_0} \frac{\mathbf{r} - \mathbf{r}'}{|\mathbf{r} - \mathbf{r}'|^2} \quad (3.17)$$

To extract the singularity, consider the dielectric interface of Figure 3.5. Substituting (3.15) into (3.10) yields

$$\begin{aligned} \mathbf{E}(\mathbf{r}) &= -\nabla \int_C \sigma_T(\mathbf{r}') \{G^p(\mathbf{r}|\mathbf{r}') + G^s(\mathbf{r}|\mathbf{r}')\} dl' \\ &= \mathbf{E}^p(\mathbf{r}) + \mathbf{E}^s(\mathbf{r}) \end{aligned} \quad (3.18)$$

where in the limit  $\mathbf{r} \rightarrow \mathbf{r}'$ , only the primary term  $\mathbf{E}^p(\mathbf{r})$  involves integration over the singularity. Bringing the  $\nabla$  operator inside the integral sign to the Green's function, we may write the primary electric field term in the following manner.

$$\begin{aligned}
\mathbf{E}^p(\mathbf{r}) &= \frac{1}{2\pi\epsilon_0} \nabla \int_C \sigma_T(\mathbf{r}') \ln |\mathbf{r} - \mathbf{r}'| dl' \\
&= \frac{1}{2\pi\epsilon_0} \lim_{\Delta c \rightarrow 0} \left[ \int_{C-\Delta c} \sigma_T(\mathbf{r}') \frac{\mathbf{r} - \mathbf{r}'}{|\mathbf{r} - \mathbf{r}'|^2} dl' + \int_{\Delta c} \sigma_T(\mathbf{r}') \nabla \ln |\mathbf{r} - \mathbf{r}'| dl' \right]
\end{aligned} \tag{3.19}$$

Only the integration over  $\Delta c$  involves the singular point  $\mathbf{r} = \mathbf{r}'$ . Let us write  $\nabla G^p(\mathbf{r}|\mathbf{r}')$  in terms of the unit normal and unit tangent vectors on  $\Delta c$ .

$$\begin{aligned}
\nabla \ln |\mathbf{r} - \mathbf{r}'| &= \frac{\partial}{\partial n} (\nabla \ln |\mathbf{r} - \mathbf{r}'|) \hat{n} + \frac{\partial}{\partial t} (\nabla \ln |\mathbf{r} - \mathbf{r}'|) \hat{t} \\
&= \frac{1}{|\mathbf{r} - \mathbf{r}'|} \left[ \frac{\partial |\mathbf{r} - \mathbf{r}'|}{\partial n} \hat{n} + \frac{\partial |\mathbf{r} - \mathbf{r}'|}{\partial t} \hat{t} \right] \\
&= \frac{1}{|\mathbf{r} - \mathbf{r}'|} [\hat{n} \cos \theta + \hat{t} \sin \theta]
\end{aligned} \tag{3.20}$$

If we assume  $\sigma_T(\mathbf{r}')$  and the unit vectors  $\hat{n}$  and  $\hat{t}$  are constant over the interval  $\Delta c$ , we obtain

$$\lim_{\Delta c \rightarrow 0} \int_{\Delta c} \sigma_T(\mathbf{r}') \nabla \ln |\mathbf{r} - \mathbf{r}'| dl' = \lim_{\Delta c \rightarrow 0} \sigma_T \left\{ \hat{n} \int_{\Delta c} \frac{\cos \theta}{|\mathbf{r} - \mathbf{r}'|} dl' + \hat{t} \int_{\Delta c} \frac{\sin \theta}{|\mathbf{r} - \mathbf{r}'|} dl' \right\} \tag{3.21}$$

The assumption that  $\hat{n}$  and  $\hat{t}$  are constant vectors over  $\Delta c$  is valid since we will be approximating all interfaces in a piece-wise linear manner. To evaluate the two right hand side integrals of (3.21), let us consider the geometry of Figure 3.6. Here, for a small angle  $d\phi$ , we obtain the following geometric relationship

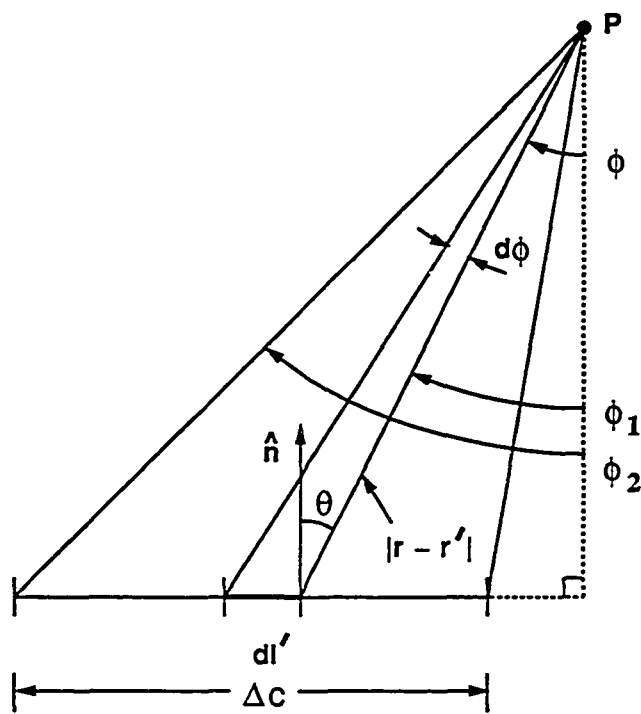


Figure 3.6: Geometry relating  $\Delta c$  and the observation point  $P$

$$dl' = \frac{|\mathbf{r} - \mathbf{r}'|}{\cos \theta} d\phi \quad (3.22)$$

Thus the two right hand side integrals of (3.21) are

$$\int_{\Delta c} \frac{\cos \theta}{|\mathbf{r} - \mathbf{r}'|} dl' = \Omega \quad (3.23)$$

$$\begin{aligned} \int_{\Delta c} \frac{\sin \theta}{|\mathbf{r} - \mathbf{r}'|} dl' &= \int_{\phi_1}^{\phi_2} \tan \phi d\phi \\ &= \frac{1}{\cos \phi_2} - \frac{1}{\cos \phi_1} \end{aligned} \quad (3.24)$$

where  $\Omega$  is the angle subtended by  $\Delta c$  as seen from the observation point  $P$ . In the limit as  $\mathbf{r} \rightarrow \mathbf{r}'$  and as  $\Delta c \rightarrow 0$ , the right hand side integrals of (3.21) become

$$\lim_{\mathbf{r} \rightarrow \mathbf{r}'} \left\{ \lim_{\Delta c \rightarrow 0} \int_{\Delta c} \frac{\cos \theta}{|\mathbf{r} - \mathbf{r}'|} dl' \right\} = \pm \pi \quad (3.25)$$

$$\lim_{\mathbf{r} \rightarrow \mathbf{r}'} \left\{ \lim_{\Delta c \rightarrow 0} \int_{\Delta c} \frac{\sin \theta}{|\mathbf{r} - \mathbf{r}'|} dl' \right\} = 0 \quad (3.26)$$

where the sign in (3.25) depends on whether we approach the boundary from the positive or negative side, respectively. Note that the positive side is defined to be the region into which  $\hat{n}$  points.

At this point, from (3.15) in view of (3.22) and (3.23), we may write the primary field at a point approaching the dielectric boundary as

$$\mathbf{E}^{p\pm}(\mathbf{r}) = \frac{1}{2\pi\epsilon_0} \text{Pr} \int_c \sigma_T \frac{\mathbf{r} - \mathbf{r}'}{|\mathbf{r} - \mathbf{r}'|^2} dl' \pm \hat{n} \frac{\sigma_T(\mathbf{r})}{2\epsilon_0} \quad (3.27)$$

for  $\mathbf{r} \in C$  and where  $\text{Pr} \int$  denotes the Cauchy principle value of the integral.

In general, for our system of conductors and dielectric-dielectric interfaces, the electric field at point  $\mathbf{r}$  on one of the dielectric-dielectric interfaces becomes

$$\mathbf{E}^\pm(\mathbf{r}) = - \sum_{j=1}^N \text{Pr} \int_{c_j} \sigma_T(\mathbf{r}') \nabla G(\mathbf{r}|\mathbf{r}') d\mathbf{l}' \pm \hat{n} \frac{\sigma_T(\mathbf{r}')}{2\epsilon_1} \quad (3.28)$$

for  $\mathbf{r} \in C_i$ ,  $i = N_c + 1, N_c + 2, \dots, N$ , and where  $\epsilon_1$  represents the dielectric constant of the planar region in which a given non-planar region of  $\epsilon_2$  resides.

Let us now apply continuity of the normal component of the electric flux at the non-planar dielectric interfaces. Substituting (3.28) into (3.14), we have

$$\begin{aligned} & -\epsilon_1 \sum_{j=1}^N \text{Pr} \int_{c_j} \sigma_T(\mathbf{r}') \nabla G(\mathbf{r}|\mathbf{r}') \cdot \hat{n} d\mathbf{l}' + \frac{\sigma_T(\mathbf{r}')}{2} \\ & = -\epsilon_2 \sum_{j=1}^N \text{Pr} \int_{c_j} \sigma_T(\mathbf{r}') \nabla G(\mathbf{r}|\mathbf{r}') \cdot \hat{n} d\mathbf{l}' - \frac{\sigma_T(\mathbf{r}')\epsilon_2}{2\epsilon_1} \end{aligned} \quad (3.29)$$

Simplifying, we have

$$\frac{\epsilon_1 + \epsilon_2}{2\epsilon_1(\epsilon_1 - \epsilon_2)} \sigma_T(\mathbf{r}) - \sum_{j=1}^N \text{Pr} \int_{c_j} \sigma_T(\mathbf{r}') \nabla G(\mathbf{r}|\mathbf{r}') \cdot \hat{n} d\mathbf{l}' = 0 \quad (3.30)$$

Substituting the approximations of  $\sigma_T(\mathbf{r})$  and  $\sigma_T(\mathbf{r}')$  into the above expression yields the second set of equations.

$$\frac{\epsilon_1 + \epsilon_2}{2\epsilon_1(\epsilon_1 - \epsilon_2)} \sigma_T(\mathbf{r}) - \sum_{j=1}^N \sum_{l=1}^{M_j} \sigma_{Tl}^{(j)} \text{Pr} \int_{\Delta c_l^{(j)}} \nabla G(\mathbf{r}|\mathbf{r}') \cdot \hat{n} d\mathbf{l}' = 0 \quad (3.31)$$

This represents our second set of equations which completes the matrix approximation of the problem.

The full matrix formulation may be written in the convenient form of

$$\sum_{j=1}^N \sum_{l=1}^{M_j} \sigma_l^{(j)} Z_{k_i l_j} = \begin{cases} V_i & i = 1, 2, \dots, N_c \\ 0 & i = N_c + 1, \dots, N \end{cases} \quad (3.32)$$

where

$$Z_{k_i l_j} = \begin{cases} \int_{\Delta C_i^{(j)}} G(\mathbf{r}|\mathbf{r}') dl' & i = 1, 2, \dots, N_c \\ - \int_{\Delta C_i^{(j)}} \nabla G(\mathbf{r}|\mathbf{r}') \cdot \hat{n} dl' & \begin{cases} i = N_c + 1, \dots, N \\ k \neq l \text{ or } i \neq j \end{cases} \\ \frac{\epsilon_1 + \epsilon_2}{2\epsilon_1(\epsilon_1 - \epsilon_2)} - Pr \int_{\Delta C_i^{(j)}} \nabla G(\mathbf{r}|\mathbf{r}') \cdot \hat{n} dl' & \begin{cases} i = N_c + 1, \dots, N \\ k = l \text{ and } i = j \end{cases} \end{cases} \quad (3.33)$$

This system of equations may be written matrix form as

$$\begin{bmatrix} [Z_{11}] & [Z_{12}] & \cdots & [Z_{1N}] \\ [Z_{21}] & [Z_{22}] & \cdots & [Z_{2N}] \\ \vdots & \vdots & \ddots & \vdots \\ [Z_{N1}] & [Z_{N2}] & \cdots & [Z_{NN}] \end{bmatrix} \begin{bmatrix} [\sigma_1] \\ [\sigma_2] \\ \vdots \\ [\sigma_N] \end{bmatrix} = \begin{bmatrix} [V_1] \\ [V_2] \\ \vdots \\ [0] \end{bmatrix} \quad (3.34)$$

where the individual  $Z_{ij}$  matrices are of dimension  $M_i \times M_j$ , the  $\sigma_j$  are  $M_j \times 1$  vectors and the  $V_i$  are  $M_i \times 1$  vectors.

To simplify the implementation of (3.34), a global numbering system is useful. Again, we have  $N$  interfaces, of which  $i = 1, 2, \dots, N_c$  represent conductor

surfaces and  $i = N_c + 1, N_c + 2, \dots, N$  represent the dielectric-dielectric interfaces. Each of these interfaces has  $M_i$  subsections. Hence a global system  $Z\sigma = V$  may replace the previous

$$\begin{bmatrix} Z_{11} & Z_{12} & \cdots & Z_{1,ntot} \\ Z_{21} & Z_{22} & \cdots & Z_{2,ntot} \\ \vdots & \vdots & \ddots & \vdots \\ Z_{ntot,1} & Z_{ntot,2} & \cdots & Z_{ntot,ntot} \end{bmatrix} \begin{bmatrix} \sigma_1 \\ \sigma_2 \\ \vdots \\ \sigma_{ntot} \end{bmatrix} = \begin{bmatrix} V_1 \\ V_2 \\ \vdots \\ 0 \end{bmatrix} \quad (3.35)$$

where  $ntot$  denotes the total number of subsections on all interfaces. In (3.35), every subinterval is individually numbered. Notice that  $\sigma$  is the total charge density on all subintervals due to one conductor charged to 1 volt while all others are grounded. This process must be repeated for every conductor being alone 1 volt in order to obtain the capacitance matrix. Although the system  $Z\sigma = V$  must be solved  $N_c$  times, the  $Z$  matrix is always the same, thus it need only be constructed once.

### 3.2 Calculation of the Per Unit Length Capacitance, Inductance and Conductance Matrices

Losses in dielectric material result in a complex permittivity,  $\epsilon$ ,

$$\epsilon = \epsilon' - j\epsilon'' \quad (3.36)$$

The effect of a lossy medium appears in the space domain Green's function, where a complex permittivity gives rise to complex coefficients  $A_i$  and  $B_i$ . For a MTL in a lossy medium, the resulting  $Z$  will be complex, consequently the  $\sigma$  matrices are also complex

$$[\sigma] = [\sigma_R] + j[\sigma_I] \quad (3.37)$$

Let us now introduce a complex  $N_c \times N_c$  matrix  $[\hat{C}]$ . In the lossless case, the p.u.l capacitance is related to the p.u.l charge matrix by the electrostatic expression

$$[Q] = [C][V] \quad (3.38)$$

However, since  $[\hat{Q}]$  and thus  $[\hat{C}]$  are complex,  $[\hat{C}]$  does not represent the p.u.l capacitance matrix with which we are familiar. Let us rewrite the above electrostatic expression as

$$[\hat{Q}] = [\hat{C}][V] \quad (3.39)$$

The individual  $\hat{C}_{ij}$  elements may be thought of as the total complex capacity of the  $i^{th}$  conductor due to the  $j^{th}$  conductor being charged to 1 volt. In terms of the complex charge density components  $\sigma_i^k$ , the elements of the  $\hat{C}$  matrix are

$$\hat{C}_{ij} = \sum_{k=1}^{M_i} \frac{\epsilon(\mathbf{r})}{\epsilon_i} \sigma_i^k \Delta l_i^k \quad (3.40)$$

Now that  $[\hat{C}]$  is known, we may write our admittance matrix in the following form [13].

$$\begin{aligned} Y &= j\omega\hat{C} \\ &= j\omega[\hat{C}_R + j\hat{C}_I] \end{aligned}$$



$$\begin{aligned}
&= -\omega\hat{C}_I + j\omega\hat{C}_R \\
&= G + j\omega C
\end{aligned} \tag{3.41}$$

Therefore, our p.u.l. capacitance and conductance matrices are given by

$$C = \hat{C}_R \tag{3.42}$$

$$G = -\omega\hat{C}_I \tag{3.43}$$

For lossless lines, we can express the p.u.l. inductance matrix in terms of the free space capacitance matrix, that is the capacitance matrix obtained by replacing the multi-dielectric medium with free space [1].

$$L = \frac{1}{c^2}[C_0]^{-1} \tag{3.44}$$

## CHAPTER 4

### Numerical Results

A Fortran program was written to calculate transmission line parameters using the previously described method. The input data consists of the locations of ground planes and dielectric layers, a pointwise representation of conductor-dielectric and dielectric-dielectric interfaces, and the dielectric constants and loss tangents at the frequency of interest. The program provides the p.u.l. capacitance, inductance and conductance matrices. In the following sections, a number of examples are presented to illustrate the accuracy and the ability of the method to handle complicated dielectric structures.

#### 4.1 MTL in a Uniform Layered Medium

In this example, we have three conducting lines in a three layered dielectric medium. Two of the lines have rectangular cross-section while the third has a circular cross-section. Each of the rectangular lines is discretized into 12 subintervals while the circular line is approximated by a 12 sided polygon. This configuration is shown in Figure 4.1. The numerical results are given in Table 4.1.

The number of subintervals per conductor for this example were chosen in order to compare with the cited references. For rectangular conductor cross sections, three subintervals per side is usually sufficient for accurate results. More subintervals may be used, but the slight increase in accuracy may not warrant the increased computation time. The exception to this is the case where one

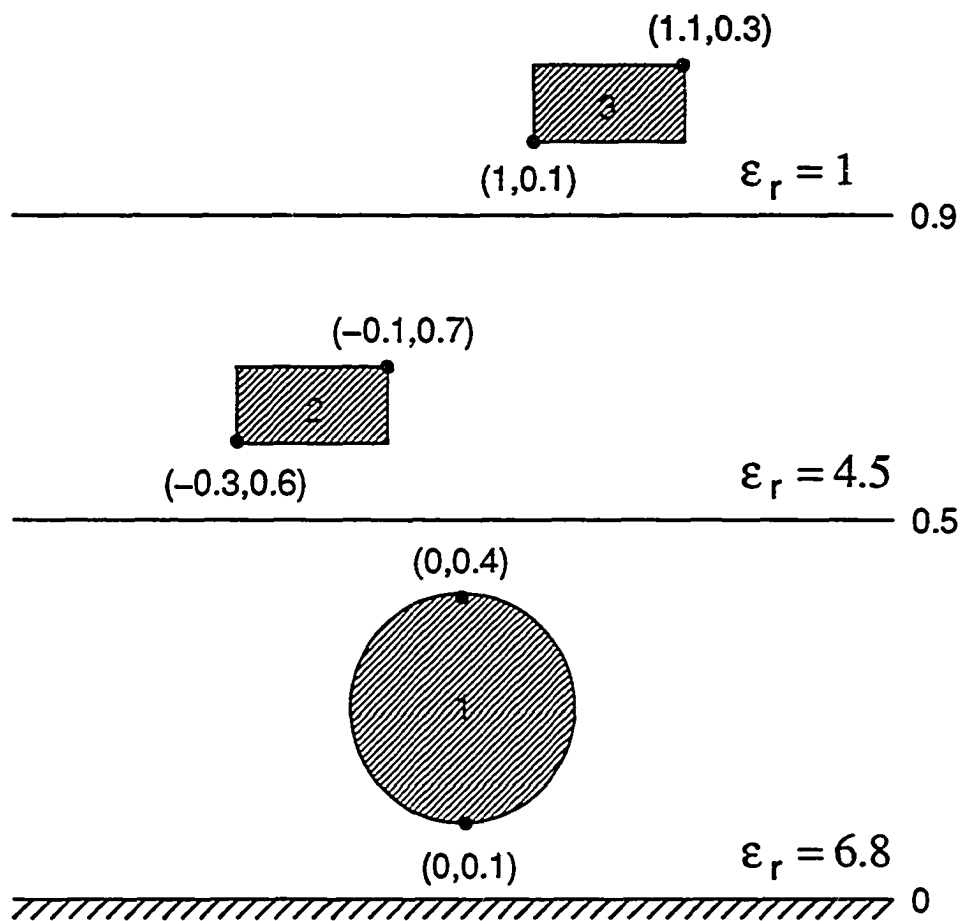


Figure 4.1: Three Conducting Lines in a Three Layered Medium

	RESULTS	REFERENCE [1]	REFERENCE [2]	UNITS
$C_{11}$	3.457	3.410	3.523	pF/cm
$C_{12}$	-0.691	-0.696	-0.683	
$C_{13}$	-0.071	-0.072	-0.072	
$C_{22}$	1.267	1.259	1.244	
$C_{23}$	-0.136	-0.131	-0.130	
$C_{33}$	0.348	0.341	0.338	
$L_{11}$	2.370	2.299	2.331	nH/cm
$L_{12}$	1.198	1.175	1.183	
$L_{13}$	0.785	0.768	0.773	
$L_{22}$	4.918	4.919	4.965	
$L_{23}$	1.985	1.989	1.996	
$L_{33}$	5.962	6.128	6.163	

Table 4.1: Results for the MTL in a Uniform Layered Medium Example.

conductor lies directly above another, thus shielding the upper conductor from the ground plane. In this case, it has been found necessary to increase the number of subintervals on the horizontal sides of the conductor. For this type of problem, six to eight subintervals on the horizontal sections of the conductor surfaces will produce accurate results.

## 4.2 Dielectric Coated Wires

Consider the two-wire ribbon configuration of Figure 4.2. This ribbon consists of two identical wires coated with a dielectric. Each of the circular interfaces is approximated by a twelve-sided polygon. For the conductor-dielectric interfaces, only one subsection per side is used. For the dielectric-dielectric interfaces, three subintervals per side are used. In calculating the capacity of the ribbon, one of the wires is assumed active while the other is grounded.

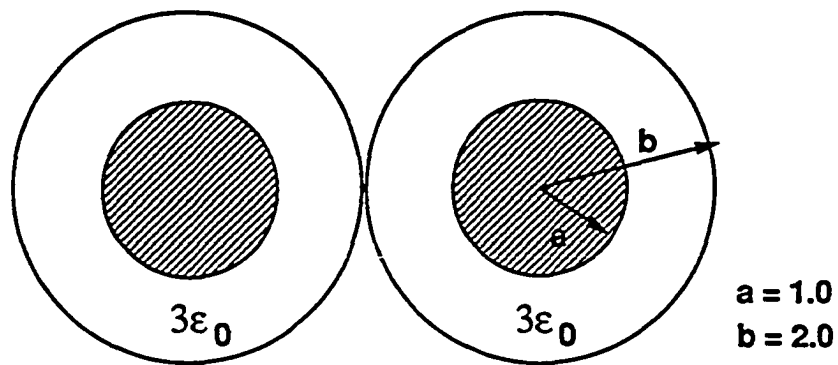


Figure 4.2: Two-wire Ribbon

	RESULTS	REFERENCE [7]	UNITS
CAPACITANCE <i>Without dielectric</i>	0.2238	0.225	pF/cm
CAPACITANCE <i>with dielectric</i>	0.4012	0.400	pF/cm

Table 4.2: Results for Two-wire Ribbon with and without the dielectric coating present

### 4.3 Dielectric Coated Microstrip Line

Consider the microstrip structure of Figure 4.3. This microstrip is thinly coated with a dielectric material. The conductor surface is discretized into twelve subsections. The dielectric coating is actually modeled as a thin layer intersecting the conductor, on which we add a small hump over the top of the line. The dielectric-dielectric interface between the hump and air is a piecewise linear approximation of 12 subsections. The calculated capacitance of this line, with and without the dielectric coating, is given in Table 4.3.

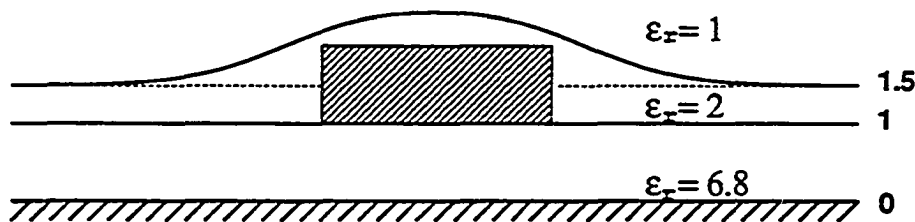


Figure 4.3: Dielectric Coated Microstrip Line

	RESULTS		Units
	w/o coating	w/ coating	
Capacitance	2.487	2.565	pF/cm
Inductance	2.013	2.011	nH/cm

Table 4.3: Results for the Microstrip Line with and without the dielectric coating

### 4.4 Differential Lines in the Presence of a Vertical Dielectric Interface

Consider a pair of differential lines in the multi-dielectric medium of Figure 4.4. Here, we are concerned with the variation in the self and coupling capacitances of the lines when the vertical dielectric interface between dielectrics 1 and 2 is

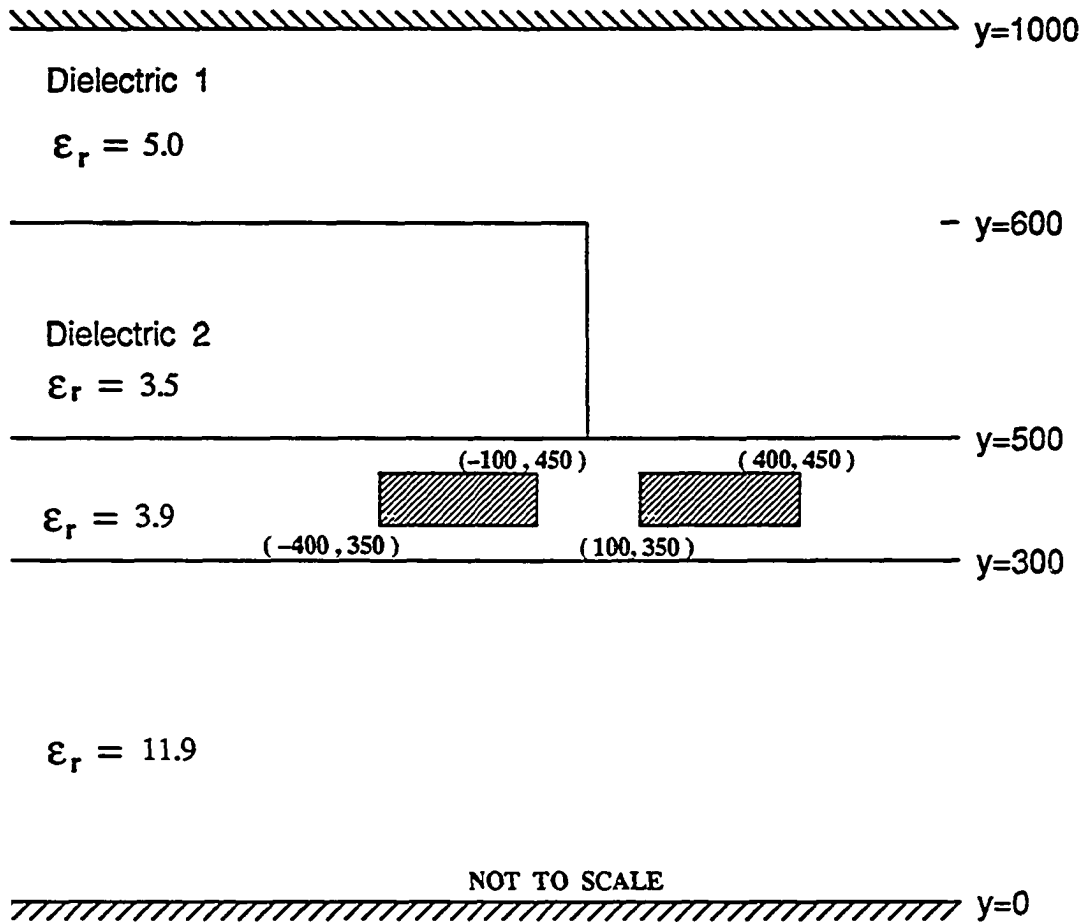


Figure 4.4: Differential lines in the presence of a vertical dielectric interface

introduced. Each conductor is discretized into 20 subintervals while the dielectric-dielectric interface is divided into 36 subintervals. The results with and without the vertical dielectric interface are given in Table 4.4.

	RESULTS		UNITS
	w/o <i>Diel.2</i>	w/ <i>Diel.2</i>	
$C_{11}$	1.9289	1.8741	pF/cm
$C_{12}$	-0.3544	-0.3538	
$C_{22}$	1.9289	1.9147	
$L_{11}$	3.5816	3.5816	nH/cm
$L_{12}$	0.8751	0.8751	
$L_{22}$	3.5816	3.5816	

Table 4.4: Results for the Differential Lines with and without DIELECTRIC 2 present



## CHAPTER 5

### Computation Time

The time required to calculate the p.u.l. capacitance and inductance matrices varies depending on whether the kernel of the integral equation is the free space Green's function or the layered medium Green's function. Given the same number of unknowns, the free space method is much faster than the layered medium method. However, as dielectric layers are added, the number of unknowns required for the free space method increase. For the layered medium method, the number of unknowns remain the same as the number of dielectric layers increases.

#### 5.1 CPU time Comparison Between Methods

Consider the single conductor line of Figure 5.1. The single conductor is discretized into 12 subsections. For the free space method, each dielectric layer interface extends from -8.0 to 8.0 in the x-direction and is subdivided into 20 subsections. As the number of layers is increased, Figure 5.2 shows how the number of unknowns differ between methods. As the number of unknowns  $N$  increases, the number of elements of the matrix increases at the rate  $N^2$ . Consequently, the time required to construct and invert the matrix is also increased. Figure 5.3 compares the CPU time between the methods as the number of layers is increased. Beyond three layers, the CPU time required for the free space method exceeds that required for the layered medium method for one conductor problem. For many conductor problems however, the free space method will generally result in lower CPU times.

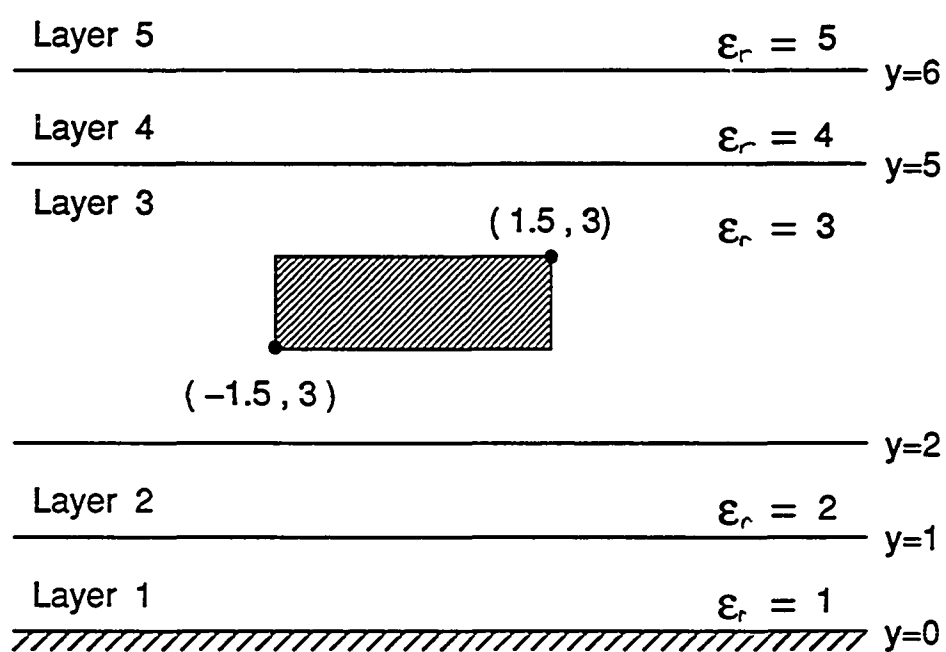


Figure 5.1: Single Conducting Line in a Multilayered Medium

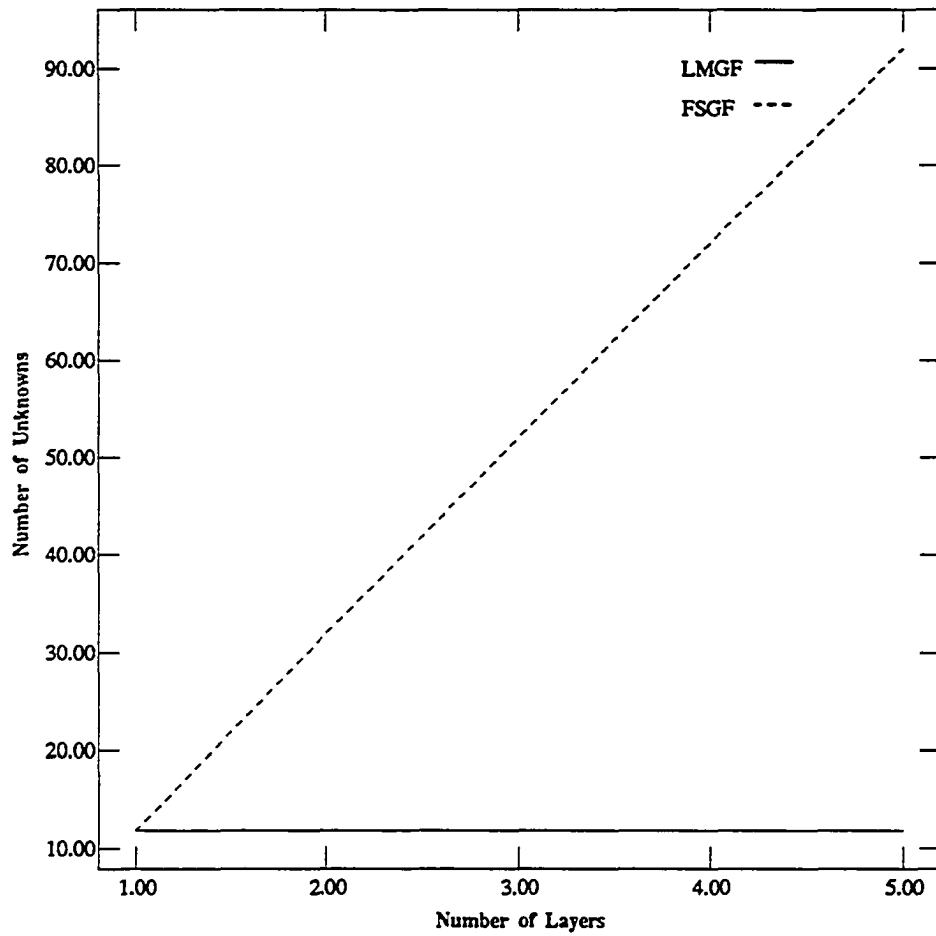


Figure 5.2: Comparison of number of unknowns between methods

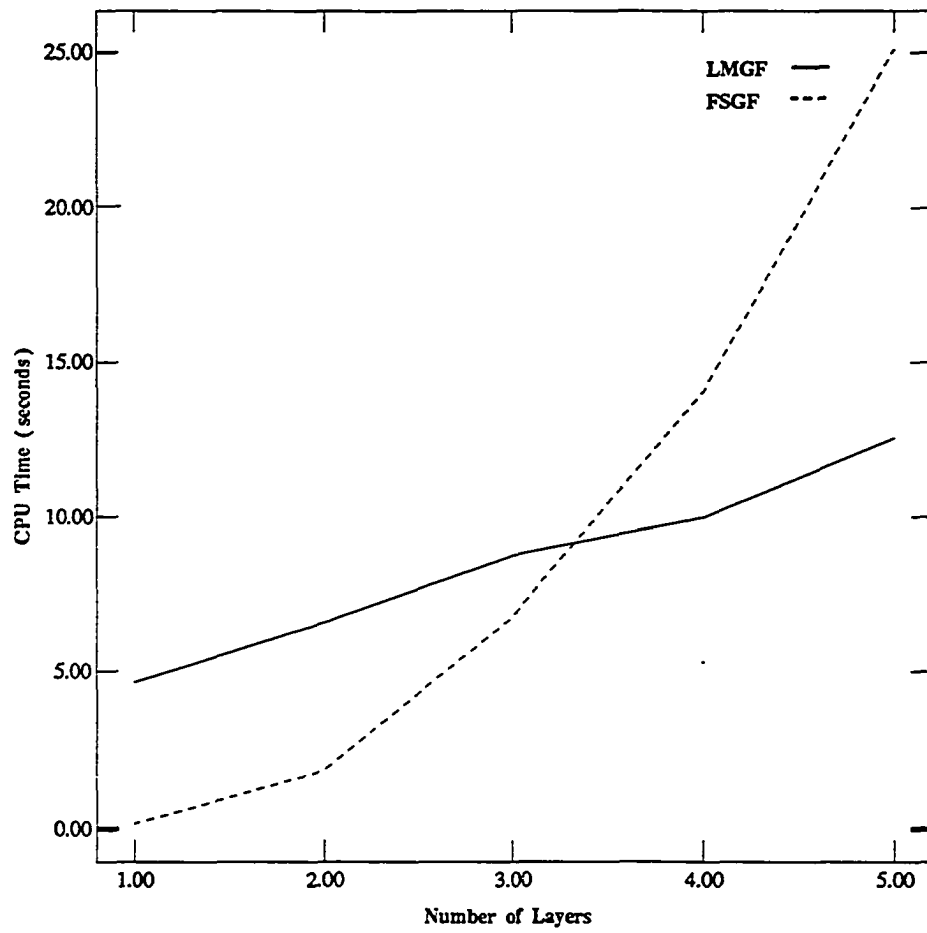


Figure 5.3: Comparison of CPU time between methods

## CHAPTER 6

### Conclusions and Future Directions

In this thesis, a method for computing the p.u.l. capacitance  $[C]$ , conductance  $[G]$ , and inductance  $[L]$  matrices for multiconductor lines in a multi-dielectric medium was presented. The formulation is quasi-TEM based on an integral equation solution of Poisson's equation for the electrostatic potential. The kernel of the integral is the Green's function for a layered dielectric medium from a paper by W. Delbale, et al. The integral equation was solved numerically using the method of moments while applying potential boundary conditions at conductor surfaces and continuity of the normal electric flux at non-planar dielectric interfaces. The solution of the system was in terms of the free charge distribution on the conductor surfaces and the polarization charge distribution on the non-planar dielectric interfaces. The direct result is the capacitance matrix where the element  $C_{ij}$  represents the sum of all the free charge on the  $i^{th}$  conductor surface while the  $j^{th}$  conductor is active and all others are grounded. When lossy dielectrics are included, the conductance matrix for the multiconductor transmission line is obtained in terms of the imaginary part of the capacitance calculation. The inductance matrix is then determined using a TEM expression in terms of the free space capacitance matrix.

The multi-dielectric medium that we can handle consists of both planar and non-planar dielectric regions. Therefore, this method may be useful in the effects of thin dielectric layers and other irregular shaped dielectric interfaces on transmission line parameters and properties such as cross-talk and characteristic impedance. A Fortran program was written and several examples were considered.

The first two examples are used to show that the transmission line parameters calculated using this method are consistent with examples found in the literature. Later examples are used to show the variety of problems which may be considered using the program. Comparisons of the CPU time of the program with methods using the free space Green's function as the kernel of the integral equation were made. Here, it was shown that as the number of dielectric layers was increased, the number of unknowns differ greatly between the methods and at some point the CPU time required to calculate the matrices using the free space Green's function method exceeds this program.

Finally, it appears the methods described here could easily be extended to three dimensional structures in a medium of uniform dielectric layers and irregular dielectric boundaries. The spectral domain Green's function could be applied to the uniform layered medium and hence the Green's function in three dimensions would be the double inverse transform of the spectral domain Green's function.

## APPENDIX A

### The Exponential Integral

The complex Exponential Integral function  $E_1(z)$  is defined as

$$E_1(z) = \int_z^\infty \frac{e^{-t}}{t} dt, \quad |\arg z| < \pi \quad (\text{A.1})$$

where  $z = x + iy$ . Here, we assume that the path of integration does not include the origin and does not cross the negative real axis. For numerical computations, the following series expansion is used.

$$E_1(z) = -\gamma - \ln z - \sum_{n=1}^{\infty} \frac{(-1)^n z^n}{nn!}, \quad |\arg z| < \pi \quad (\text{A.2})$$

where  $\gamma = 0.5772156649$  is Euler's constant. The symmetry relation for the Exponential Integral is

$$E_1(\bar{z}) = \overline{E_1(z)} \quad (\text{A.3})$$

From a practical standpoint, (A.2) is not useful for large complex arguments since the rate of convergence is much slower. For  $|x| > 10$  or  $|y| > 10$ , it is convenient to use the following approximation [15].

$$e^z E_1(z) = \frac{0.711093}{z + 0.415775} + \frac{0.278518}{z + 2.29428} + \frac{0.010389}{z + 6.2900} + \epsilon(z), \quad \epsilon(z) < 3 \times 10^{-6} \quad (\text{A.4})$$

## APPENDIX B

### The Cosine Integral

The complex Cosine Integral function is defined as

$$Ci(z) = - \int_z^\infty \frac{\cos t}{t} dt, \quad |\arg z| < \pi \quad (\text{B.1})$$

where  $z = x + iy$ . Again, the path of integration is assumed to exclude the origin and does not cross the negative real axis. The real Cosine Integral function, which for the reason just stated is valid only for positive real arguments, is

$$Ci(x) = - \int_x^\infty \frac{\cos t}{t} dt, \quad x > 0 \quad (\text{B.2})$$

The series expansion of the real cosine integral function is given by

$$Ci(x) = \gamma + \ln x + \sum_{n=1}^{\infty} \frac{(-1)^n x^{2n}}{2n(2n)!} \quad (\text{B.3})$$

For large arguments, it is more practical to write the cosine integral in terms of the auxiliary functions  $f(x), g(x)$ .

$$Ci(x) = f(x) \sin x + g(x) \cos x \quad (\text{B.4})$$

The auxiliary functions themselves are defined in term of the sine and cosine integral functions, however for numerical purposes, we may use rational approximations of  $f(x)$  and  $g(x)$ . For  $f(x)$ , we have



$$f(x) = \frac{1}{x} \left( \frac{x^8 + a_1 x^6 + a_2 x^4 + a_3 x^2 + a_4}{x^8 + b_1 x^6 + b_2 x^4 + b_3 x^2 + b_4} \right) + \epsilon(x), \quad 1 \leq x < \infty$$

$$|\epsilon(x)| < 5 \times 10^{-7}$$

$$\begin{aligned} a_1 &= 38.027264 & b_1 &= 40.021433 \\ a_2 &= 265.187033 & b_2 &= 322.624911 \\ a_3 &= 335.677320 & b_3 &= 570.236280 \\ a_4 &= 38.102495 & b_4 &= 157.105423 \end{aligned} \tag{B.5}$$

For  $g(x)$ , we have

$$g(x) = \frac{1}{x^2} \left( \frac{x^8 + a_1 x^6 + a_2 x^4 + a_3 x^2 + a_4}{x^8 + b_1 x^6 + b_2 x^4 + b_3 x^2 + b_4} \right) + \epsilon(x), \quad 1 \leq x < \infty$$

$$|\epsilon(x)| < 3 \times 10^{-7}$$

$$\begin{aligned} a_1 &= 42.242855 & b_1 &= 48.196927 \\ a_2 &= 302.757865 & b_2 &= 482.485984 \\ a_3 &= 352.018498 & b_3 &= 1114.978885 \\ a_4 &= 21.821899 & b_4 &= 449.690326 \end{aligned} \tag{B.6}$$

## APPENDIX C

### Numerical Evaluation of Singular Integrals

Consider the integral

$$I = \int_{-1}^1 f(\eta) d\eta \quad (\text{C.1})$$

where the function  $f(\eta)$  is singular at a point  $\bar{\eta}$  in the interval of integration. A non-linear transformation is available which places quadrature points closely around the singularity, thus providing a more accurate numerical integration than standard Gaussian quadrature [11].

Let us consider a third order non-linear transformation of the form

$$\eta(\gamma) = a\gamma^3 + b\gamma^2 + c\gamma + d \quad (\text{C.2})$$

for which we impose the following constraints

$$\frac{d\eta}{d\gamma} \Big|_{\bar{\eta}} = 0 \quad (\text{C.3})$$

$$\frac{d^2\eta}{d^2\gamma} \Big|_{\bar{\eta}} = 0 \quad (\text{C.4})$$

$$\eta(1) = 1 \quad (\text{C.5})$$

$$\eta(-1) = -1 \quad (\text{C.6})$$

Condition (C.3) implies an extrema at  $\bar{\eta}$  while (C.4) implies that the Jacobian of the transformation has an extrema at  $\bar{\eta}$ . The resulting solution of the transformation is

$$\eta = \frac{(\gamma - \bar{\gamma})^3 + \bar{\gamma}(\bar{\gamma}^2 + 3)}{1 + 3\bar{\gamma}^2} \quad (\text{C.7})$$

$$d\eta = \frac{3(\gamma + \bar{\gamma})^2}{1 + 3\bar{\gamma}^2} d\gamma \quad (\text{C.8})$$

where  $\bar{\gamma}$  is the value of  $\gamma$  for which  $\eta(\bar{\gamma}) = \bar{\eta}$ . This may be determined by

$$\bar{\gamma} = [\bar{\eta}^3 - \bar{\eta}^2 + |\bar{\eta}^2 - 1|]^{1/3} + [\bar{\eta}^3 - \bar{\eta}^2 - |\bar{\eta}^2 - 1|]^{1/3} + \bar{\eta} \quad (\text{C.9})$$

Once this transformation is performed, standard Gaussian quadrature is used to evaluate the integral. Note that the integral of (C.1) has already been transformed to the interval  $[-1,1]$ . This must be done in order to apply the non-linear transform discussed in this section.

## REFERENCES

- [1] C. Wei, R.F. Harrington, J.R. Mautz and T.K. Sarkar, "Multiconductor transmission lines in multilayered dielectric media," *IEEE Trans. Microwave Theory Tech.*, vol. MTT-32, pp. 439–449, April 1984.
- [2] W. Delbare and D. DeZutter, "Space domain Green's function approach to the capacitance calculation of multiconductor lines in multilayered dielectrics with improved surface charge modeling," *IEEE Trans. Microwave Theory Tech.*, vol. MTT-37, pp. 1562–1568, October 1989.
- [3] W.T. Weeks, "Calculation of coefficients of capacitance of multiconductor transmission lines in the presence of a dielectric interface," *IEEE Trans. Microwave Theory Tech.*, vol. MTT-18, pp. 35–43, January 1970.
- [4] E. Yamashita, "Variational method for the analysis of microstrip-like transmission lines," *IEEE Trans. Microwave Theory Tech.*, vol. MTT-16, pp. 529–535, Aug, 1968.
- [5] S.R.H. Hoole, *Computer Aided Analysis and Design of Electromagnetic Devices*, Elsevier, New York, 1989.
- [6] O. Palusinski, *ECE 556 Course Notes: Principles of Packaging*, University of Arizona, 1991.
- [7] C.C. Clements, C.R. Paul and A.T. Adams, "Computation of the capacitance matrix for systems of dielectric-coated cylindrical conductors," *IEEE Trans. on Electromagnetic Compatibility*, vol. EMC-17, pp. 238–248, November 1975.
- [8] G. Arfken, *Mathematical Methods for Physicists*, Academic press, Orlando, 1985.

- [9] R.F. Harrington, *Field Computations by Method of Moments*, Macmillan, New York, 1968
- [10] J.R. Brews, "Electrical modeling of interconnections," *Submicron Integrated Circuits*, Wiley, New York, 1989.
- [11] J.F.C. Telles, "A self adaptive co-ordinate transformation for efficient numerical evaluation of general boundary element integrals," *International Journal For Numerical Methods In Engineering*, "vol 24, pp. 959-973, 1987.
- [12] J.R. Wait, *Electromagnetic Wave Theory*. Harper & Row, New York, 1985
- [13] P.A. Rizzi, *Microwave Engineering*. Prentice-Hall, New Jersey, 1988
- [14] M. Abramowitz and I. Stegun, Eds., *Handbook of Mathematical Functions*, Washington, DC: National Bureau of Standards, 1965.
- [15] J. Todd, "Evaluation of the exponential integral for large complex arguments," *J. Research NBS*, vol 52, pp. 313-317, 1954